INVESTIGATION OF COUPLED AXIAL-LATERAL-TORSIONAL DRILLSTRING VIBRATIONS USING A MULTI-BODY DYNAMICS APPROACH

by

© Ehsan Fallahi

A thesis submitted to the

School of Graduate Studies

in partial fulfillment of the requirements for the degree of

Master of Engineering

Faculty of Engineering and Applied Science

Memorial University of Newfoundland

May 2014

St. John's Newfoundland

ABSTRACT

Drillstring vibration is a very crucial phenomenon which has a great effect on the drilling process. The drillstring is responsible to transfer rotary motion and energy to the drill bit. Unwanted vibration causes reduction in the rate of penetration (ROP), bit wear and connection failure between drillstring parts. In this thesis, a model of a realistic drill collar is generated which can predict any possible motion of the drill collar.

This study contains several analyses about drillstring vibration in three main modes. The focus is on the drill collar section of the drillstring because of the importance of this section in vibration generation of the whole drillstring. This study attempts to determine the vibration behavior of the drill collar in axial, lateral and torsional directions in the presence of vibration-assisted rotary drilling (VARD) and unbalanced rotation.

The model includes self weight, hydraulic forces due to drilling mud circulation and most realistic boundary condition for each particular scenario. This model also can be used for coupled vibration states and determination of vibration behavior of the drillstring in three coupled modes, simultaneously. Simulation results show the vibration behavior of the drillstring due to several cases and boundary conditions. The time response to each single mode is expressed and will be validated by finite element method (FEM). The vibration behavior of the rotating drillstring in three coupled modes will be studied using unbalanced rotation of the drillstring. The rock-bit interaction will also be applied to the model. Finally, the effect of the VARD tool will be examined.

ACKNOWLEDGEMENTS

I would like to express my sincere gratitude to my graduate supervisors, Dr. Stephen Butt and Dr. Geoff Rideout for their constant guidance, encouragement and great support which gave me the opportunity to do this research.

I would like to thank Mr. Farid Arvani, the project manager for his support and encouragement.

I would also thank the Atlantic Canada Opportunity Agency, Husky Energy, and Suncor Energy, Faculty of Engineering and Applied Science for providing financial support for this research.

My special thanks to Moya Crocker for her supervision and help.

I would like to dedicate this thesis to my kind parents, Ebrahim and Fariba for their endless support.

Table of Contents

List of Tables

List of Figures

List of Symbols, Nomenclature or Abbreviations

A	Cross Section Area
BHA	Bottom-hole assembly
C	Compliance
CG	Center of Gravity
d	Diameter
E	Modulus of Elasticity
e	Effort
F	Net External Force
f	Flow
F_x	Net External Force in x direction
F_y	Net External Force in y direction
F_z	Net External Force in z direction
g	Gravity Acceleration
GY	Gyrator
h	Angular Momentum
I	Inertial Element
J	Polar Moment of Inertia
J_x	Polar Moment of Inertia in x direction
J_y	Polar Moment of Inertia in y direction
J_z	Polar Moment of Inertia in z direction
l	Length

MGY	Modulated Gyrator
MTF	Modulated Transformer
P	Translational Momentum
P_x	Translational Momentum in x direction
P_y	Translational Momentum in y direction
P_z	Translational Momentum in z direction
R	Resistance Element
r	Radius
ROP	Rate of Penetration
Se	Source of Effort
TF	Transformer
TOB	Torque on Bit
V	Translational Velocity
VARD	Vibration Assisted Rotary Drilling
V_x	Translational Velocity in x direction
V_y	Translational Velocity in y direction
V_z	Translational Velocity in z direction
WOB	Weight on Bit
X	Horizontal Axis (perpendicular to Y) in Global Frame
Y	Horizontal Axis in Global Frame
Z	Vertical Axis in Global Frame
x	Horizontal Axis (perpendicular to Y) in Local Frame

y	Horizontal Axis in Local Frame
z	Vertical Axis in Local Frame
ω	Angular Velocity
ω_x	Angular Velocity in x direction
ω_y	Angular Velocity in y direction
ω_z	Angular Velocity in z direction
θ	Pitch Angle
ϕ	Roll Angle
ψ	Yaw Angle
Θ	Pitch Matrix
Φ	Roll Matrix
Ψ	Yaw Matrix

List of Appendices

1. Introduction

1.1. Drilling Technology

Drilling is a most common method to explore and exploit oil and gas reservoirs. The purpose of advanced drilling techniques is to increase the rate of production as well as decrease the cost. New areas are studied to enhance drilling proficiency. Drillstring is one of the most important parts of drill rigs, for which some studies have been conducted to control the vibration of this huge structure. Drillstring is responsible to transfer the energy from the surface to the drill bit. It is obvious that controlling the unwanted vibration will result in better performance of drilling process and reduction in the exploitation cost.

The drillstring is a slender structure which transfers energy from the rotary table at the surface to the drill bit at the bottom hole. The drillstring includes two major parts: drill pipe section and drill collar section. The drill pipe is a cylindrical pipe which is relatively light and has the length up to kilometers. The drill collar section is heavier and responsible to provide weight on bit (WOB). The collar section is cylindrical and could be up to hundreds of meters. The drill pipe is under tension while the collar should be under compression due to the hoisting load and hydrostatic mud effect. The neutral point is the place in the drillstring where compression changes to tension. The drill bit is connected to the bottom of the collar. Rate of penetration (ROP) is the index to evaluate the drilling efficiency which is dependent on WOB. The drillstring undergoes three major modes of vibration: axial, torsional and lateral. These three states can be coupled via variables such as torque.

The mud which is circulated along the drillstring to the bottom hole cools the bit and flushes the cuttings. The stabilizers are connected to the collar section to prevent buckling and deviation of drilling trajectory. Bottom hole assembly (BHA) includes drill collar, drill bit and stabilizers. The vibration behavior of the drillstring strongly depends on the vibration behavior of the BHA due to higher mass and higher stiffness of the BHA with regard to the pipe section. A schematic view of a drill rig is shown in Figure 1-1.

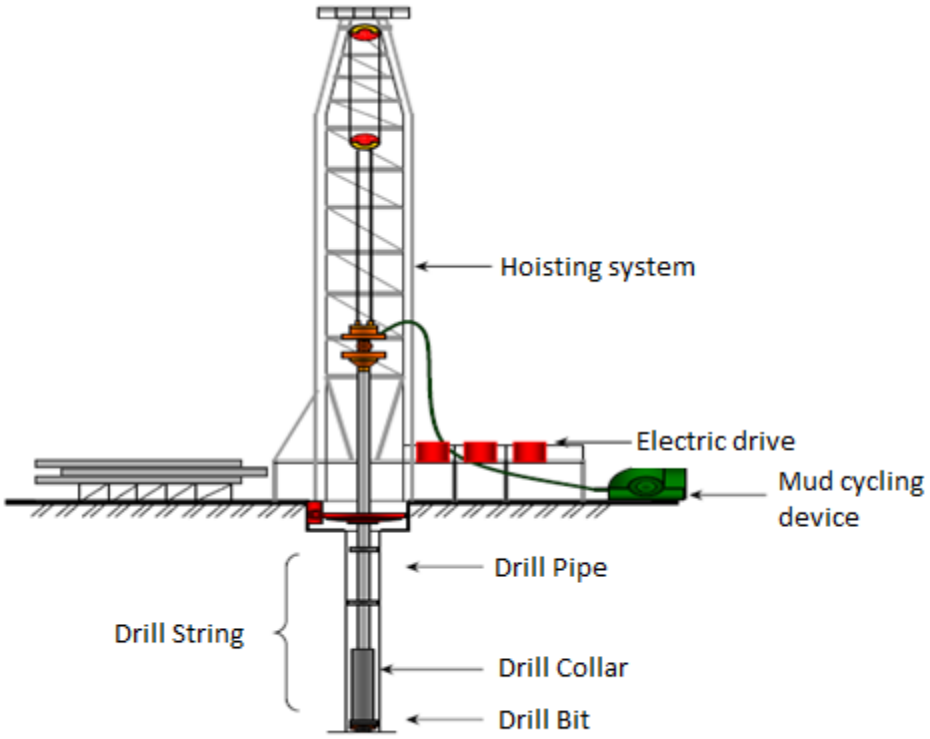

Figure 1-1 Schematic view of a drill rig (Chien-Min Liao, 2011)

Vibration assisted rotary drilling (VARD) project is a 6 year research project which studies the effect of adding vibration to conventional rotary drilling. This project includes a series of experimental and numerical investigation to improve the drilling efficiency.

There are currently a group of graduate students and faculty investigators involved in the project, to investigate different areas of the project to build a prototype. This research investigates the coupled axial-lateral and torsional vibration behavior of the drillstring. The project is led by Memorial University with Dr. S. Butt as the principal investigator and industry partnerships including RDC, Husky Energy and Suncor Energy.

1.2. Thesis statement

The drillstring is one of the crucial components in drilling rigs. The drillstring is responsible for transferring energy and rotation from rotary table at the surface to the bit at the bottom hole. So, the efficiency of drilling is very dependent on the drillstring dynamic behavior. It is a long and slender structure which is subjected to spatially axial loads and torque. Axial loads include distributed self weight of the drillstring, buoyant effect due to the mud circulation and hoisting load at the surface.

The drillstring is under three major states of vibration. Axial, torsional and lateral are the three main modes which can occur in the drillstring. Moreover, these three modes can be coupled together because of interaction terms such as torque. Axial-transverse,

axial-torsional, and torsional-transverse are examples of coupled mode vibration in the drillstring. These unwanted vibrations have severe effect on the drilling process. Reduction in the rate of penetration, bit wear, and failure in the joints are some examples of drillstring vibration drawbacks.

Weight on bit (WOB) is the result of the interaction of axial loads which provides the cutting force at the lower end of the drillstring. Vibration assisted rotary drilling (VARD) tool implements the vibration to the WOB to increase the drilling efficiency. Bit-rock interaction, and contact with the wellbore are main sources of excitation of the vibration modes. Lateral vibration has the most destructive effect on the drillstring between the three main modes. It is because of the lower traveling speed of the lateral waves along the drillstring. The lateral vibration of the drill pipe can be neglected since it is not excited in the lower modes. The drill collar can be excited in lower modes because it is always under compression and it has lower natural frequencies (Gabriel *et al.*, 1997; Berlioz *et al.*, 1996; Kriesels *et al.*, 1999). To prevent lateral vibration of the collar, stabilizers are used in this section.

To mitigate the unwanted vibration of the drillstring, the dynamic behavior of the drillstring should be studied and revealed. Isolation methods can be implemented when a comprehensive study of the drillstring vibration is done and potential vibration behaviors are anticipated.

Currently, to the best of author's knowledge, there is no study to investigate the axial-lateral-torsional vibration behavior of the drillstring, simultaneously. In this research, a dynamic model capturing coupled axial-torsional and lateral vibration of the

drillstring will be developed. A series of nonlinear multi-dynamic equations for a rigid body in 3-D will be developed and then a bond graph model of this rigid body will be constructed. Using the bond graph lumped segment method and a series of compliances and dampers, a model with as many elements as desired will be introduced.

Using multibody dynamic approach, a 3-D body in the bond graph will be developed. For simulating the drillstring, 30 segments will be aligned and a series of springs and dampers will be introduced to connect segments, to make a continuous rod. Validation will be done using Finite Element Method (FEM). The same model will be constructed in Abaqus (ABAQUS Theory Manual (version 6.10), 2012, Dassault Systèmes Simulia Corp., RI, USA).

The coupled axial-lateral and torsional vibration behavior of the drillstring will be investigated under several conditions such as VARD tool and unbalanced rotation. The goal of this research is to develop a fast-running, physically intuitive model which is easy to expand to include features such as VARD tool, shuck sub and wellbore contact.

2. Literature review on drillstring vibrations

2.1. Three main modes of vibration in the drillstring

Drillstring vibration has been a big issue for drillers in oil fields for a long time. Drillstring undergoes major damage, such as, fatigue, joint failure, and instability due to the unwanted vibration and these drawbacks have made drilling companies look for ways to control the drillstring vibration and mitigate these effects to obtain higher performance with less cost (Wiercigroch *et al.*, 2008; Han *et al.*, 2006). To do this, the behavior of the drillstring vibration should be studied and modeled analytically (Bailey *et al.*, 2008; Spanos *et al.*, 1992; Ghasemloonia *et al.*, 2012), experimentally (Khulief *et al.*, 2009) and through field verification (Jogi *et al.*, 2002).

The drillstring undergoes different kinds of vibration during the drilling operation. Axial, torsional and lateral vibrations are the main modes which occur in drillstring (Zifeng *et al.*, 2007). These three modes are shown in Figure 2-1.

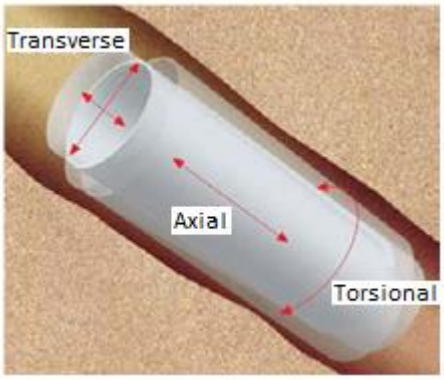

Figure 2-1 Three different modes of vibration in drillstring (Jardine *et al.*, 1994)

These modes are coupled together. The combination of vibration modes causes complicated shape modes.

2.2. Axial vibration of the drillstring

Axial or longitudinal vibrations are mostly due to the interaction between the drill bit and the rocks. Bit bouncing is a common outcome of axial vibration, as shown in Figure 2-2. It mostly happens in hard formation in vertical wells. Moreover, axial vibration is responsible for failure in measurement while drilling (MWD) tools, reduction in penetration rate (ROP), seal failure and broken tooth cutters (Ashley *et al.*, 2001).

It has been realized that axial vibration and bit bounce can be reduced by changing rotational speed or weight on bit, in some cases (Shuttleworth *et al.*, 1998). Because of the crucial role of axial vibration in well trajectory and ROP, researchers have been involved to mitigate the axial vibration as much as possible. Another suggested way is to

install a shock sub above the drill bit which changes the resonance frequency of the drillstring. The importance of shock sub to reduce the axial vibration of the drillstring was revealed by Kreisle *et al.* (1970).

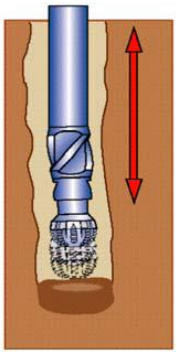

Figure 2-2 Axial vibration of the drillstring and bit bounce (Ashley *et al.*, 2001)

Researchers have used different models to study the axial vibration of the drillstring. Continuous modeling was the first approach to study the axial vibration (Dareing 1968). Recently, finite element modeling has been used to investigate axial vibration of the drillstring (Spanos *et al.*, 1995). The axial vibration investigation has been completed over the years and recent studies consider the most realistic case which includes most parts of the drillstring.

2.3. Torsional vibration of the drillstring

Torsional vibration occurs due to nonlinear interaction between the rock and the bit or drillstring with the borehole (Sananlkone *et al.*, 1992). It causes serious failure in drillstring connections, and bit, and slows down the drilling process (Elsayed *et al.*,

1997). Stick-slip interactions are the main cause of torsional vibration. Stick-slip is a severe form of torsional vibration of the drillstring. It is the result of torsional and whirling mode of the drillstring (Challamel *et al.*, 2000; Leine *et al.*, 2002). During the stick-slip oscillation, the rotational speed of the bit is varied in a wide range, from zero to twice as high as surface speed (Chen *et al.*, 1999). Figure 2-3 shows the stick-slip phenomenon of the drillstring.

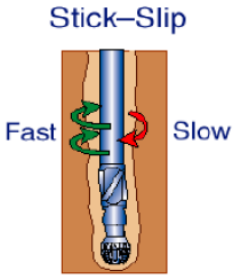

Figure 2-3 Torsional vibration of the drillstring (Ashley *et al.*, 2001)

Torsional vibration can be detected using MWD or at the surface. When the needed power to maintain the constant speed is changed, torsional vibration is happening. The most common model to study the torsional vibration is a torsional pendulum. In this model, the drill pipe is considered as a spring and bottom hole assembly (BHA) is modeled as a mass. This model has been modified over the years and more realistic cases have been considered. For example, the rotary table has been implemented to the model as another lumped mass (Lin *et al.*, 1991; Zamanian *et al.*, 2007; Abbasian *et al.*, 1998).

2.4. Transverse vibration of the drillstring

The most destructive type of drillstring vibration is lateral or transverse (Kriesels *et al.*, 1999). Bending or lateral vibrations are often caused by drill pipe eccentricity, leading to rotational motion named as drillstring whirl. Bending waves are not propagated in a drillstring as axial and torsional waves move up to the surface. This is due to high damping value of transverse mode because of mud damping effect and wellbore contact (Chin, 1994). As a result, transverse modes of the drillstring may not be detected at the surface. Figure 2-4 shows the lateral mode of the drillstring vibration.

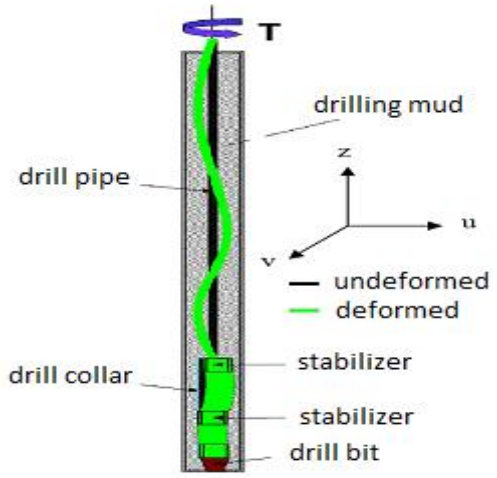

Figure 2-4 Transverse vibration of the drillstring (Khulief *et al.*, 2008)

Due to the axial load distribution, the collar section should be in compression and pipe section remains in tension. Therefore, the collar section can be excited in lower modes and natural frequency of the collar section is reduced while the natural frequency

of pipe section is increased and it does not vibrate in lower modes (Thomsen, 2003). Bit failure, borehole washout and BHA failure are the possible effects of transverse vibration (Leine *et al*., 2002).

To study the severity of lateral vibration of the drillstring, many studies have been done. Lumped segment method, Lagrangian method, transfer matrix technique and laboratory tests are examples of the previous studies (Jansen, 1991; Christoforou *et al.*, 1997; Chen *et al.*, 1995; Berlioz *et al.*, 1996).

2.5. Coupled modes vibration of the drillstring

The primary modes of vibration in the drillstring are axial, torsional and lateral. These modes can be coupled by quantities, such as WOB or TOB (Christoforou *et al.*, 2001). The three common coupled modes are coupled axial-bending; coupled torsional-bending and coupled axial-torsional (Yigit *et al.*, 1996; Yigit *et al.*, 1998; Elsayed *et al.*, 2002). Drillstring vibrations are complicated and coupled. Over the last two decades, an extensive number of modeling, simulation, and experimental studies have been conducted to understand these vibrations (Cook, Nicholson, and Westlake, 1986; Dufour, and Draoui, 1996; Yigit and Christoforou, 1998; Melakhessou, Berlioz, and Ferraris, 2003; Spanos *et al.*, 2003; van de Wouw, Rosielle, and Nijmeijer, 2007; Ritto, Soize, and Sampaio, 2009).

Kyllingstad and Halsey (1988) studied the stick-slip phenomenon associated with torsion vibration, using single degree-of-freedom (DOF) system. Berlioz *et al.* (1996)

conducted experiments to examine the coupling between bending and axial vibrations. Yigit and Christoforou (1997) focused on the coupling between lateral and axial vibrations. Using the kinetic and strain energy of the beam and Lagrange equation, the equations of motion of a non rotating drillstring were generated.

The bottom hole assembly (BHA) has been modeled as an unbalanced rotor supported by two bearings (Jansen, 1991). A four degree-of-freedom model was presented by Berlioz and Ferraris (2003) in which the bending and torsion motions of the drillstring were studied.

Complexities of torsion drillstring dynamics is presented by Leine *et al.*, (2002) when stick-slip and whirl motions are considered. Moreover, finite element analyses have been carried using linear models (Khulief, 2005; Spanos *et al.*, 2003). They did not include rotation of the drillstring in their models.

Navarro-Lopez and Cortes (2007) focused on failure in the drillstring due to axial vibrations. The effect of changing weight on bit (WOB) and rotary speed on the drillstring vibration have been studied by Richards *et al.* (2004). They concluded that undesirable oscillatory phenomena can be avoided by changing WOB and rotary speed.

Although several studies have been developed to understand axial vibrations, stick-slip phenomenon, and lateral vibrations, a comprehensive model which can treat this problem remains to be conducted. In addition, there are many nonlinear phenomena that have not been fully modeled or examined, given the complexity of the dynamics. In this study, the coupled axial-lateral-torsional vibration of a rotating drillstring will be examined.

2.6. Modeling methods

Newtonian approach

There is a relationship between the equation of motion of any mechanical dynamic system and expression of Newton's second law of motion. It can be expressed as the differential equation (Meirovitch, 1967):

$$f(t) = \frac{d}{dt}(m\frac{dr(t)}{dt})$$

where $f(t)$ is the applied force vector and $r(t)$ is the position vector of the mass *m*. If the mass does not vary with time (which is true in most structural dynamics), then:

$$f(t) - m\frac{d^2r}{dt^2} = 0$$

The term $m\frac{d^2r}{dt^2}$ is called inertia force that resists the acceleration of the mass.

This approach is a vectorial approach and uses physical coordinates to describe the motion. In Newtonian mechanics, motions are usually measured relative to an inertia reference frame. In this research, the equation of motion will be derived for translational and torsional motions.

Energy method

For analyzing the complicated systems, energy methods are preferred to the Newtonian approach because of the scalar measuring of energy variables. For the rotary coordinate system or for nonlinear systems the energy methods are preferred (Thomsen, 2003). The

energy method is not a fast running method and a small change in the system will result in changing the governing equations of the whole system. As a result, it is not an ideal method for this research which will examine many case scenarios.

Finite Element Method (FEM)

Due to the nonlinearity of a model such as coupled vibration modes, solving the model requires an approximate or numerical solution because analytical methods result in a set of coupled algebraic equations.

The first application of the FEM to the problem of drillstring vibration was by Millheim *et al.* (1978). Flexural and torsional modes were studied as two uncoupled modes without considering and gravitational effect (Axisa and Antunes, 1990). Melakhessou *et al.* (2003) used the FEM to study the contact behavior of the drillstring and the wellbore at a single contact point. Khulief *et al.* (2005) studied the rotating drillstring using the FEM. They considered both drill collars and drill pipes sections in the torsional-transverse mode. Ghasemloonia *et al.* (2012) used the FEM to study the coupled axial-transverse vibration behavior of the entire drillstring under the effect of vibration assisted rotary drilling (VARD) tool.

The objective of this study is to achieve an accurate model of the drillstring to investigate the vibration behavior of the drillstring under different conditions. The model should include mud buoyancy and damping, rotation, gravitational forces, torque, axial forces, etc. The focus will be on the collars and stabilizers section. As aforementioned in the literature review, due to the complexity of the coupled modes, currently there is no study

that investigates all three vibration modes of the drillstring simultaneously. Several modeling methods have been used, such as, FEM, energy method and Newtonian approach. To study the vibration behavior of the drillstring in coupled axial-lateral-torsional, the governing equations should be generated and solved in three dimensions. A small change in the boundary conditions or initial conditions will result in change of the governing equation of the whole model. Moreover, FEM and energy methods are not fast-running methods. Lumped method is a fast-running method and very easily expandable. First of all, a mathematical model is needed. For the governing equations, the beam element under all prescribed load can be assumed. The method of direct Newtonian approach for lumped mass are used to generate the equations of a single element. The governing equations will then be casted into commercial simulation software which makes the model easily expandable. In chapter 4, an analysis of vibration behavior is presented and the effect of VARD tool and bit-rock interaction is investigated.

3. Multi-body Dynamics

Multi-body dynamics is used to describe a rigid body in 3-D space. The governing equations will be derived using the basic Newton's law. Translational motions and angular motions will be defined separately and will be merged at the end. The resultant

equations are called Euler's equations. At the end of the day, a rigid body which has 6 degrees of freedom (DOF) is reached.

The rigid body will be casted into bond graph modeling. In the bond graph each motion can be interpreted separately and it is a fast-running model compared to the energy method and FEM. It is also easy to expand for including desired boundary condition or modeling more realistic situations.

After modeling a single 3-D body, one needs to add those bodies to build the drillstring. The whole model is made of as many single segments as desired. This method is called lumped segment method. These segments are aligned and connected via various stiffness components and dampers. The stiffness components are 3×3 matrices that depend on the size, the shape and the material type. The damping factors are 3×3 matrices that are adjusted using a Finite Element Method (FEM). Damping factors remain the same for the whole drillstring.

Finally, the desired drillstring is simulated in the bond graph. Because each motion is separated by others, boundary conditions can be implemented in any direction. For instance, the rotary table is modeled as a constant torque at the top segment and the translational motion of that point is blocked which simulates the cable and the derrick. The scope of this project is to simulate the 3-D drillstring in the bond graph which is expandable. Moreover, it will be able to catch all three vibration modes, simultaneously. The model includes self weight of the drill pipe and the drill collar, VARD tool, and bit-rock interaction. Unbalanced rotation is obtained by moving the center of gravity (COG).

Wellbore contact, mud circulation, and axial rock-bit interaction are outside the scope of this work and will be left as future work.

3.1. Euler's Equations

This chapter deals with multi-body dynamics modeling. After introducing general governing equations, we will be able to construct a system model which includes three-dimensional (3-D) rigid-body motion.

Figure 3-1 shows a general rigid body which can move either in translational or rotational directions. Axes x, y, z are attached to the center mass of the body (local coordinate) and axes X, Y, Z are inertial (global coordinate). The local frame usually is not a proper coordinate to view the body motion and it must be transformed to the inertial frame.

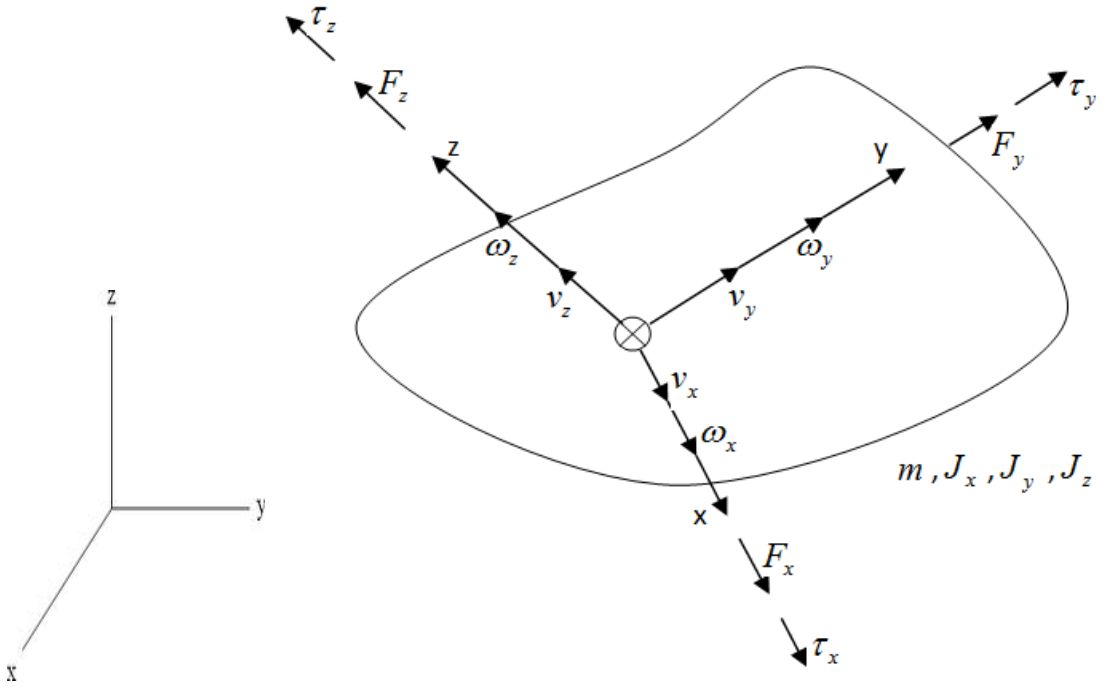

Figure 3-1 Body in general 3-D motion (Karnopp *et al.*, 2006)

The absolute velocity (v) and absolute angular velocity (ω) have been cast into three perpendicular components: v_x, v_y, v_z and $\omega_x, \omega_y, \omega_z$. These are velocities and angular velocities with respect to the rotating frame. According to Newton's law, the net force acting on the body is obtained as:

$$\vec{F} = \frac{d}{dt}\vec{P} \tag{1}$$

Where

$$P = mv \tag{2}$$

In other words,

$$F = \frac{\partial p}{\partial t}\Big|_{rel} + \omega \times p \tag{3}$$

$\frac{\partial p}{\partial t}\Big|_{rel}$ indicates the rate of change of momentum relative to an observer moving with the body-fixed frame.

An angular momentum law is analogous to equation (1). Equation (4) relates the net torque on the body to the angular momentum (*h*).

$$\tau = \frac{d}{dt} h \tag{4}$$

If the x-y-z frame is aligned with the principal axes of the body, *J* relates the angular momentum to the angular velocity:

$$h = J\omega \tag{5}$$

J is a diagonal matrix of the principal moments of inertia. *h* is defined with respect to the rotating frame, so:

$$\tau = \frac{\partial h}{\partial t}\Big|_{rel} + \omega \times h \tag{6}$$

Using the right hand rule, the components of forces and torques acting on the body can be extracted:

$$F_x = m\dot{v}_x + m\omega_y v_z - m\omega_z v_y \tag{7}$$

$$F_y = m\dot{v}_y + m\omega_z v_x - m\omega_x v_z \tag{8}$$

$$F_z = m\dot{v}_z + m\omega_x v_y - m\omega_y v_x \tag{9}$$

and

$$\tau_x = J_x\dot{\omega}_x + \omega_y J_z\omega_z - \omega_z J_y\omega_y \tag{10}$$

$$\tau_y = J_y\dot{\omega}_y + \omega_z J_x\omega_x - \omega_x J_z\omega_z \tag{11}$$

$$\tau_z = J_z\dot{\omega}_z + \omega_x J_y\omega_y - \omega_y J_x\omega_x \tag{12}$$

Equations (7) - (12) are called Euler's equations. They are nonlinear differential equations and have no general analytical solution. If they were solved numerically or analytically for a special case, $v_x, v_y, v_z, \omega_x, \omega_y, \omega_z$ would be known with respect to the local frame. Therefore, these components should be aligned with the inertial frame for better interpreting of body motion.

If the external forces and torques are considered to be inputs to the body and velocities and angular velocities are considered as outputs, the state equations can be written and the submodel is ready to be connected to any external system. Then, the overall system is modeled. With this assumption, the state equations are:

$$\dot{p}_x = F_x + m\omega_z \frac{p_y}{m} - m\omega_y \frac{p_z}{m} \tag{13}$$

$$\dot{p}_y = F_y + m\omega_x \frac{p_z}{m} - m\omega_z \frac{p_x}{m} \tag{14}$$

$$\dot{p}_z = F_z + m\omega_y \frac{p_x}{m} - m\omega_x \frac{p_y}{m} \tag{15}$$

$$\dot{p}_{j_x} = \tau_x + J_y\omega_y \frac{p_{j_z}}{J_z} - J_z\omega_z \frac{p_{j_y}}{J_y} \tag{16}$$

$$\dot{p}_{j_y} = \tau_y + J_z\omega_z \frac{p_{j_x}}{J_x} - J_x\omega_x \frac{p_{j_z}}{J_z} \tag{17}$$

$$\dot{p}_{j_z} = \tau_z + J_x\omega_x \frac{p_{j_y}}{J_y} - J_y\omega_y \frac{p_{j_x}}{J_x} \tag{18}$$

where

$$\omega_x = \frac{p_{j_x}}{J_x} \tag{19}$$

$$\omega_y = \frac{p_{j_y}}{J_y} \tag{20}$$

$$\omega_z = \frac{p_{j_z}}{J_z} \tag{21}$$

3.2. Bond Graph Method

To simulate the drillstring, bond graphs have been employed. A brief overview of bond graph modeling is presented in this section:

Bond graphs are used to describe different kinds of dynamic systems in different types of energy domains. Basically, bond graphs can model and connect different dynamic models using a single, small set of graphical elements. Elements are connected with power bonds which contain a pair of signals known as “effort” and “flow” whose product gives instantaneous power of the bond. For a mechanical system, effort and flow are force and velocity respectively, and for an electrical system they are voltage and current. Half arrows on the bonds define the direction of positive power flow. Casual strokes, placed to one end of each bond, define whether or not an element has a causal flow or effort output. Elements bounded to a 0-junction have common effort, and the algebraic sum of their flows is zero. Elements bonded to a 1-junction have common flow but their efforts algebraically sum to zero. The generation of governing equations is facilitated using bond graphs which allow prediction of numerical issues such as differential-algebraic equations and implicit.

Table 1 shows the analogies between mechanical and electrical systems in terms of effort and flow.

Table 1 Energy domains in bond graph

Variables	General	Mechanical	Electrical
Effort	$e(t)$	Force (Torque)	Voltage
Flow	$f(t)$	Velocity (Angular Velocity)	Current
Momentum	$p = \int e dt$	Momentum (Angular Momentum)	Flux linkage
displacement	$q = fdt$	Distance (Angle)	Charge
power	$P(t) = e(t) f(t)$	F(t)V(t) (τ(t)ω(t))	$e(t)i(t)$
Energy (kinetic)	$E(p) = \int f dp$	$\int V dp \quad \left(\int \omega dH\right)$	$\int id\lambda$; Magnetic
Energy(potential)	$E(q) = \int e dq$	$\int F dX \quad \left(\int \tau d\theta\right)$	$\int edq$; Electric

Mechanical, electrical and thermo-fluid systems can be modeled in bond graphs using a series of generalized energy storage, dissipation and transfer elements. Bond graph standard elements will be now explained.

R-Element:

R-element is a 1-port element in which the effort and flow variables are related by a static function. It is usually used to show energy dissipation in any kinds of system. Mechanical

dashpots or dampers, electrical resistors and orifices in fluid systems are examples of the R-Element. The bond graph symbol for the R-element is shown below.

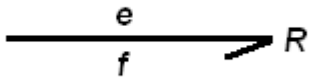

Figure 3-2 Bond graph R-element (Karnopp *et al.*, 2006)

The half arrow is always pointing towards R and it means that positive power flows into the R element. The constitutive relationship between e, f and R is given by:

$$e = \Phi_R(f)$$

C-Element:

C-element is a 1-port element in which the effort and displacement (time integral of flow) are related by a static constitutive relation. It stores and gives up energy without loss. For instance, springs, electrical capacitors, and accumulators are examples of C-elements in different systems. The bond graph symbol for the C-element is shown below.

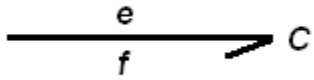

Figure 3-3 Bond graph C-element (Karnopp *et al.*, 2006)

In a spring, the deformation (x) and the effort (e) are given by:

$$x = \int f dt \ , \qquad e = \mathrm{K} \int f dt$$

In the second case, flow is the causal input and effort is the causal output.

I-Element

I-element is also a 1-port energy storing element which is also called an inertial element. It is used to simulate mass or inertia effects in mechanical systems and inductance in electrical systems. The bond graph symbol for the I-element is shown below.

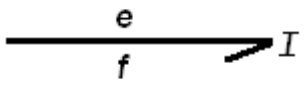

Figure 3-4 Bond graph I-element (Karnopp *et al.*, 2006)

Constitutive relationship between *e*, *f* and *R* is given by:

$$\dot{p} = e$$
$$f = \phi_I^{-1}(p)$$

Effort and Flow Sources:

Sources prescribe effort and flow from the environment, and thus enforce boundary conditions. Force is considered as effort source and velocity source gives flow source, such as, moving the surface of a rigid body. Figure 3-5 shows the effort and flow sources in bond graph.

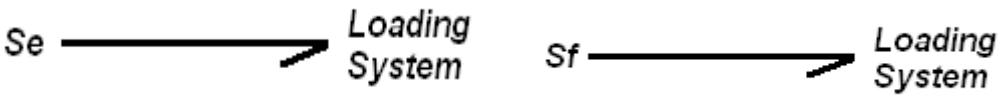

Figure 3-5 Bond graph sources

The Transformer:

The transformer does not create, store or dissipate energy. It conserves power and transmits the factor of power with proper scaling which is defined by the transformer modulus (*r*). A massless lever in mechanical domain and an electrical transformer are ideal examples of transformers. The bond graph symbol of the transformer is shown below.

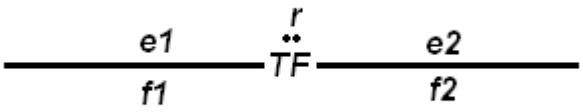

Figure 3-6 Bond graph transformer (Karnopp *et al.*, 2006)

The constitutive relationship between efforts, flows, and transformer modulus (r) is given by:

$$f_2 = r.f_1 \quad , \quad e_2 = \frac{1}{r} e_1$$

So, the conservation of power is obtained:

$$e_1 f_1 = e_2 f_2$$

The Gyrator

The Gyrator is also power conserving element which relates flow to efforts and effort to flow. The gyrator symbol in bond graph is shown in figure 3-7.

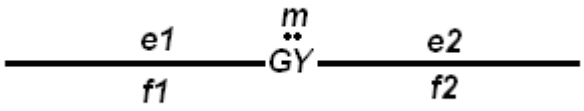

Figure 3-7 Bond graph gyrator (Karnopp *et al.*, 2006)

The constitutive relationship between efforts, flows, and gyrator modulus (*m*) is given by:

$e_2 = m.f_1$, $e_1 = m.f_2$

Similar to the transformer, the power conservation is reached:

$e_1 f_1 = e_2 f_2$

The 0- and 1-junction

There are two types of junctions which connect elements in bond graphs. They conserve power and are reversible.

- Zero junction (0): elements with equal efforts (*e*) connect to this junction and the algebraic summation of flows (*f*) is zero. This junction represents a mechanical series and electrical node point.

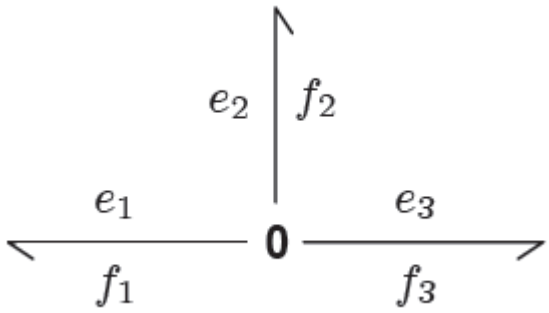

Figure 3-8 Bond graph 0-junction (Karnopp *et al.*, 2006)

The constitutive relation for Figure 3-8 can be written as follows:

$$e_1 f_1 + e_2 f_2 + e_3 f_3 = 0$$

As 0-junction is an effort equalizing junction,

$$e_1 = e_2 = e_3$$

This leads to:

$$f_1 + f_2 + f_3 = 0$$

The signs in the algebraic sum are determined by half-arrow directions in a bond graph.

- One junction (1): elements with equal flows (*f*) connect to this junction and the algebraic summation of efforts is zero. Such a junction represents a common mass point in a mechanical system and a series connection (same current flowing) in an electrical system.

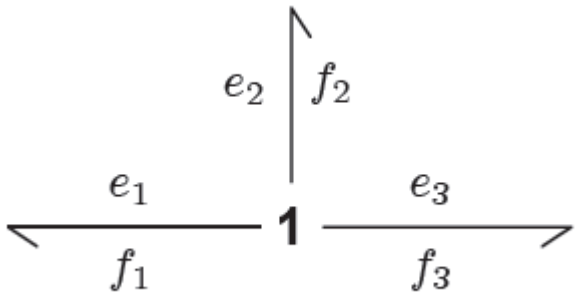

Figure 3-9 Bond graph 1-junction (Karnopp *et al.*, 2006)

In this case, the constitutive relation becomes,

$$e_1 f_1 + e_2 f_2 + e_3 f_3 = 0$$

As 1-junction is a flow equalizing junction,

$$f_1 = f_2 = f_3$$

Therefore,

$$e_1 + e_2 + e_3 = 0$$

The signs in the algebraic sum are determined by half-arrow directions in a bond graph.

Causality

A bond links two elements, one of which sets the effort and the other one the flow. The causality assignment procedure chooses who sets what for each bond. It is necessary to transform the bond graph into state space equations which is a computable code. In bond graphs, the inputs and the outputs are characterized by the causal stroke. It establishes the

cause and effect relationship between the factors of power. Figures 3-10 and 3-11 show two causal strokes in bond graphs:

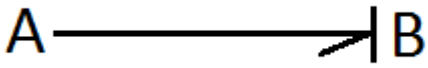

Figure 3-10 Causal stroke: A sets *e* and B sets *f*

Figure 3-11 Causal stroke: B sets *e* and A sets *f*

For 0-junction, one of the bonds sets the effort for the rest, so only one causal stroke is on the junction, while the others are away from it. For 1-junction, one of the bonds sets the flow for rest and its effort is computed from them, so all but one of the causal strokes are on the junction, while the remaining one is away from it. Sources set either the flow or the effort, so only one causality is possible. Energy storage elements, *I* or *C*, have a preferred causality in which the computation involving integrals instead of derivatives. This is called integral causality. *C*-elements are given the flow and return the effort, while I-elements are given the effort and return the flow. For these elements, differential causality is possible but not desirable because the response to a step input will be unbounded. However, it is sometimes unavoidable. For *R*-elements, causality can be set

by the rest of the system, so it is an element with indifferent causality. In Figure 3-12, the causality of bond graph elements are depicted.

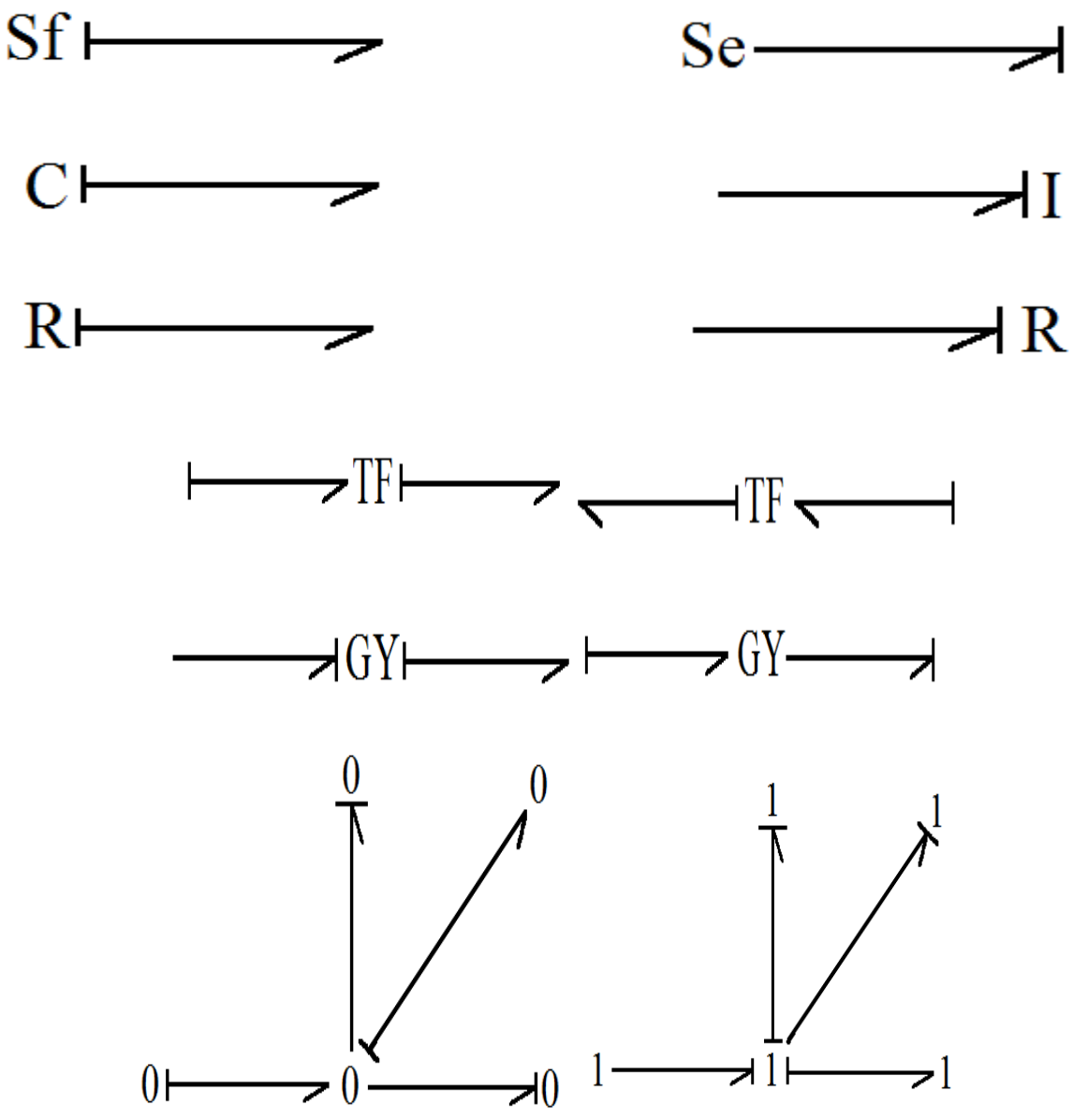

3-12 Causality of the bond graph elements

The following is an example of analogies between two basic mechanical and electrical systems:

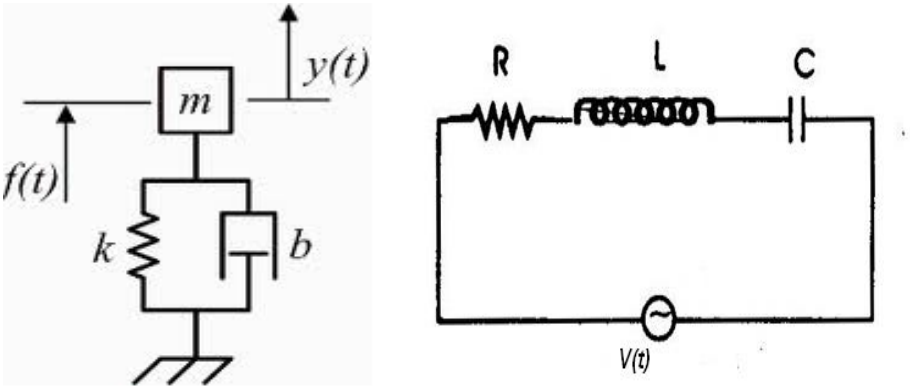

Figure 3-13 Two analogous systems (mass-spring-damper and resistance-inductance-capacitor)

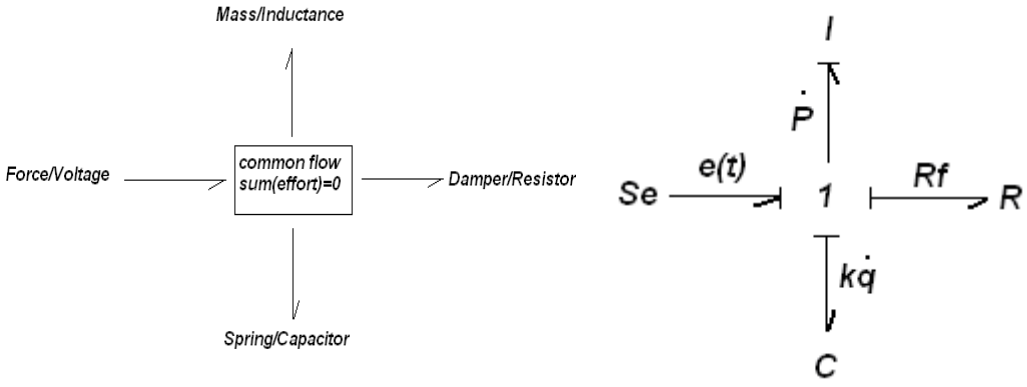

Figure 3-14 Word bond graph and full bond graph of two analogous systems

Multi and vector bond graphs

In the case of similarities in sub-system components in a model, they can be represented in a concise form called vector or multi bond graphs. They are drawn as two parallel lines with power directions. In another word, they are compact form of huge systems with identical sub-systems. All the sub-systems must have same power and causal stroke structure.

3.3. Bond graph modeling of the Euler's equations

A series of nonlinear dynamic equations in 3-D were developed for translational and angular motion. In this section, we construct the bond graph model for these two sets of equations. Equations (13)-(15), the translational motion of a rigid body in bond graph is represented by the following:

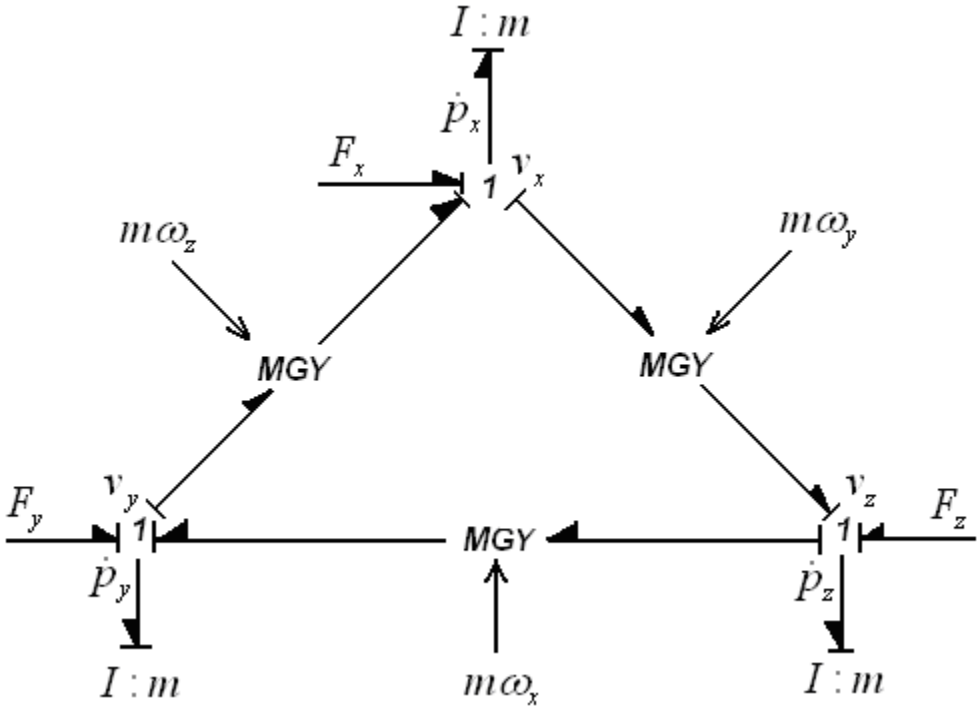

Figure 3-15 Bond graph model for a rigid body in 3-D (translational)

Similar to the translational motion, Figure 3-16 is illustrating the angular motion in 3-D for a rigid body.

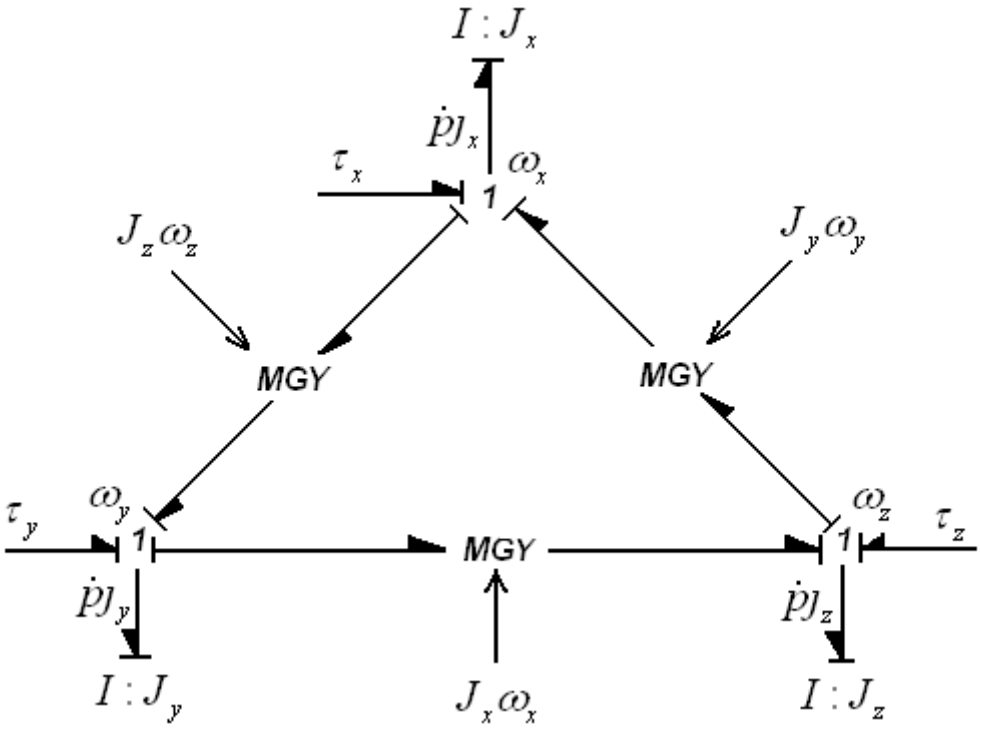

Figure 3-16 Bond graph for a rigid body in 3-D (angular motion)

3.4. Coordinate Transformation

Since it is difficult to interpret body motion in body-fixed frame as continuous change of principal directions, it is necessary to transfer from local coordinate to the global coordinate through a series of coordinate transformations. Coordinate transformation is needed to apply vectors like gravity which have inertial directions. Also, defining a joint constraint between two elements is facilitated by coordinate transformation. To plot positioning, we need to integrate velocity components in an inertial frame. Cardan angles will be used to make this transformation. Figure 3-17 shows the yaw, pitch and roll

angles. The inertial frame (X, Y, Z) rotates about Z through angle ψ (yaw). The developed orientation is named (x', y', z') axes. This coordinates then is rotated about y'-axis through the angle θ (pitch), yielding the (x'', y'', z'') axes. Finally, (x'', y'', z'') frame is rotated about x''-axis through the angle ϕ (roll). The achieved coordinate is the instantaneous body-fixed frame (x, y, z).

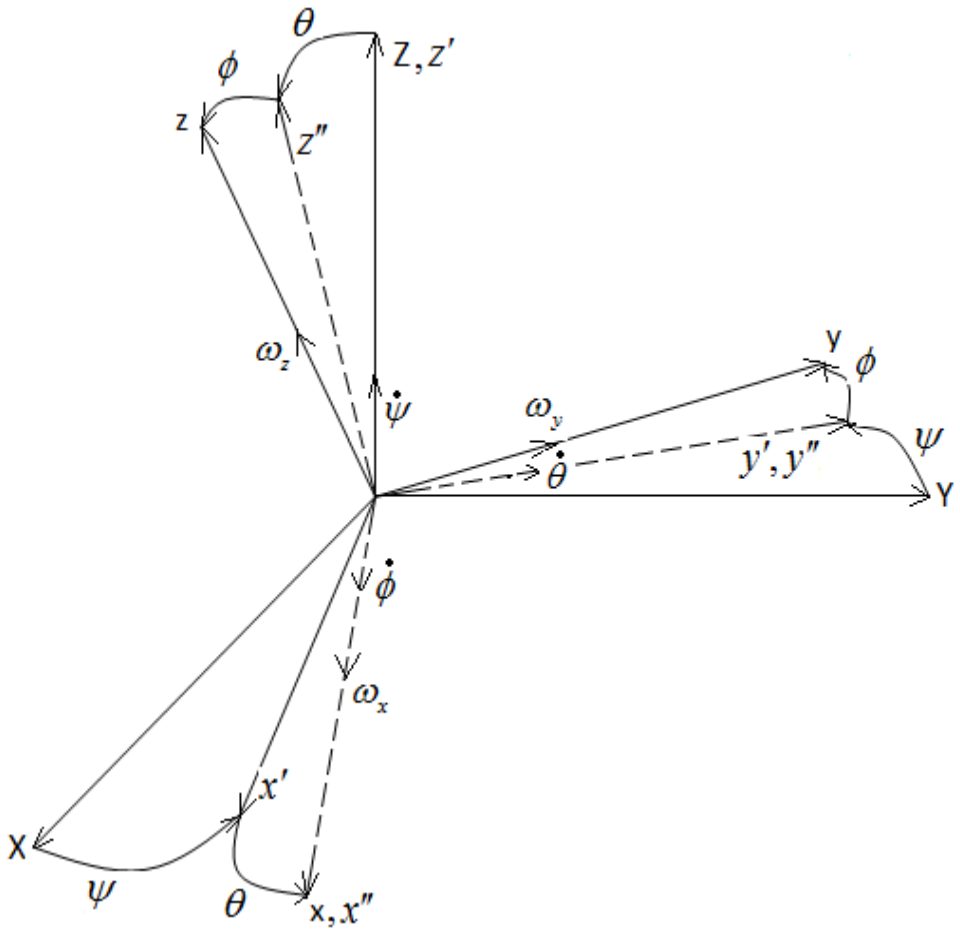

Figure 3-17 Cardan angle coordinate transformation (Karnopp *et al.*, 2006)

To clearly show how to transform from the local frame to the inertial frame, here is an example for the angular velocity.

$$\omega_{x''} = \omega_x \tag{22}$$

$$\omega_{y''} = \omega_y \cos\phi - \omega_z \sin\phi \tag{23}$$

$$\omega_{z''} = \omega_y \sin\phi + \omega_z \cos\phi \tag{24}$$

$$\omega_{x'} = \omega_{x''} \cos\theta + \omega_{z''} \sin\theta \tag{25}$$

$$\omega_{x'} = \omega_{x''} \cos\theta + \omega_{z''} \sin\theta \tag{25}$$

$$\omega_{y'} = \omega_{y''} \tag{26}$$

$$\omega_{z'} = -\omega_{x''} \sin\theta + \omega_{z''} \cos\theta \tag{27}$$

$$\omega_X = \omega_{x'} \cos\psi - \omega_{y'} \sin\psi \tag{28}$$

$$\omega_Y = \omega_{x'} \sin\psi + \omega_{y'} \cos\psi \tag{29}$$

$$\omega_Z = \omega_{z'} \tag{30}$$

In matrix form:

$$\begin{bmatrix} \omega_{x''} \\ \omega_{y''} \\ \omega_{z''} \end{bmatrix} = \begin{bmatrix} 1 & 0 & 0 \\ 0 & \cos\phi & -\sin\phi \\ 0 & \sin\phi & \cos\phi \end{bmatrix} \begin{bmatrix} \omega_x \\ \omega_y \\ \omega_z \end{bmatrix} \tag{31}$$

$$\begin{bmatrix} \omega_{x'} \\ \omega_{y'} \\ \omega_{z'} \end{bmatrix} = \begin{bmatrix} \cos\theta & 0 & \sin\theta \\ 0 & 1 & 0 \\ -\sin\theta & 0 & \cos\theta \end{bmatrix} \begin{bmatrix} \omega_{x''} \\ \omega_{y''} \\ \omega_{z''} \end{bmatrix} \tag{32}$$

$$\begin{bmatrix} \omega_X \\ \omega_Y \\ \omega_Z \end{bmatrix} = \begin{bmatrix} \cos\psi & -\sin\psi & 0 \\ \sin\psi & \cos\psi & 0 \\ 0 & 0 & 1 \end{bmatrix} \begin{bmatrix} \omega_{x'} \\ \omega_{y'} \\ \omega_{z'} \end{bmatrix} \tag{33}$$

As a result, if the angular velocities are known in the body-fixed frame, then the angular velocity component can be derived in inertial frame as well as intermediate frames.

Let us introduce the transformation matrices as:

$$\Phi = \begin{bmatrix} 1 & 0 & 0 \\ 0 & \cos\phi & -\sin\phi \\ 0 & \sin\phi & \cos\phi \end{bmatrix} \tag{34}$$

$$\Theta = \begin{bmatrix} \cos\theta & 0 & \sin\theta \\ 0 & 1 & 0 \\ -\sin\theta & 0 & \cos\theta \end{bmatrix} \tag{35}$$

$$\Psi = \begin{bmatrix} \cos\psi & -\sin\psi & 0 \\ \sin\psi & \cos\psi & 0 \\ 0 & 0 & 1 \end{bmatrix} \tag{36}$$

Then we can easily write:

$$\begin{bmatrix} \omega_X \\ \omega_Y \\ \omega_Z \end{bmatrix} = \Psi\Theta\Phi \begin{bmatrix} \omega_x \\ \omega_y \\ \omega_z \end{bmatrix} \tag{37}$$

Translational velocities have the same relationship as angular velocities. Therefore, we have the same matrix form for translational velocities:

$$\begin{bmatrix} v_X \\ v_Y \\ v_Z \end{bmatrix} = \Psi\Theta\Phi \begin{bmatrix} v_x \\ v_y \\ v_z \end{bmatrix} \tag{38}$$

Moreover, the transformation is power-conserving, since no energy is stored or dissipated by the transformation components. Therefore, one can use the same transformation matrices to convert forces and torques, as well.

$$\begin{bmatrix} F_x \\ F_y \\ F_z \end{bmatrix} = (\Psi\Theta\Phi)^T \begin{bmatrix} F_X \\ F_Y \\ F_Z \end{bmatrix} \tag{39}$$

$$\begin{bmatrix} \tau_x \\ \tau_y \\ \tau_z \end{bmatrix} = (\Psi\Theta\Phi)^T \begin{bmatrix} \tau_X \\ \tau_Y \\ \tau_Z \end{bmatrix} \tag{40}$$

The advantage of this model is to take forces and torques in inertial coordinate and align these efforts to instantaneous principal directions. Then, by integrating the first order equations, it can give the velocities and angular velocities in the local frame or instantaneous principal directions. The last step is transforming these local velocities through Cardan angles to the velocities in inertial directions.

To do these, we have to derive the Cardan angles by relating $\dot{\phi}, \dot{\theta}$ and $\dot{\psi}$ to angular velocities in body-fixed coordinate ($\omega_x, \omega_y, \omega_z$).

We have

$$\omega_x = \dot{\phi} - \dot{\psi}\sin\theta \tag{41}$$

$$\omega_y = \dot{\theta}\cos\phi + \dot{\psi}\cos\theta\sin\phi \tag{42}$$

$$\omega_z = -\dot{\theta}\sin\phi + \dot{\psi}\cos\theta\cos\phi \tag{43}$$

If equations (41)-(43) are solved for $\dot{\theta}$ and $\dot{\psi}$, then:

$$\dot{\phi} = \omega_x + \sin\phi \frac{\sin\theta}{\cos\theta}\omega_y + \cos\phi \frac{\sin\theta}{\cos\theta}\omega_z \tag{44}$$

$$\dot{\psi} = \frac{\sin\phi}{\cos\theta}\omega_y + \frac{\cos\phi}{\cos\theta}\omega_z$$

$$\dot{\theta} = \cos\phi.\omega_y - \sin\varphi.\omega_z$$

3.5. Submodel of one element in bond graph

The governing equations for one body, which are known as Euler's equations, were derived and the coordinates and corresponding transformation were introduced. The goal is to put these equations together and construct the corresponding bond graph which can predict the motion in 3-D directions. It should be mentioned that the total degrees of freedom of such a model is 6:

- Axial motion along the Z axis
- Lateral motion in X and Y directions
- Angular motion about the Z axis
- Angular motion about X and Y axes

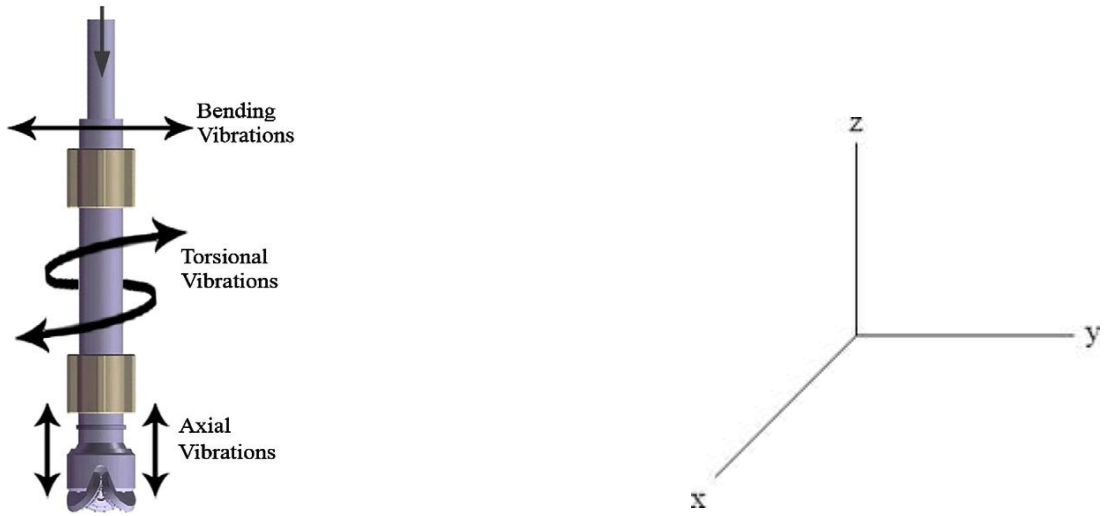

Figure 3-18 Degrees of freedom of the submodel (Hakimi, H. *et al.*, 2010)

We are now ready to build a single 3-D body in bond graph. Each body has two hinges at the top and bottom. The bottom hinge of one body will be connected to the top hinge of the next body.

The two bond graph models for translational and angular motions were already shown. Now, this model includes all motions in a single bond graph. Equations (10) - (12) can be rewritten in the following matrix form:

$$\begin{bmatrix}\tau_x\\ \tau_y\\ \tau_z\end{bmatrix}=\begin{bmatrix}J_x & 0 & 0\\ 0 & J_y & 0\\ 0 & 0 & J_z\end{bmatrix}\begin{bmatrix}\dot{\omega}_x\\ \dot{\omega}_y\\ \dot{\omega}_z\end{bmatrix}+\begin{bmatrix}0 & -\omega_z J_y & \omega_y J_z\\ \omega_z J_x & 0 & -\omega_x J_z\\ -\omega_y J_x & \omega_x J_y & 0\end{bmatrix}\begin{bmatrix}\omega_x\\ \omega_y\\ \omega_z\end{bmatrix} \quad (45)$$

The second term is simplified as:

$$\begin{bmatrix} 0 & -\omega_z & \omega_y \\ \omega_z & 0 & -\omega_x \\ -\omega_y & \omega_x & 0 \end{bmatrix} \begin{bmatrix} J_x & 0 & 0 \\ 0 & J_y & 0 \\ 0 & 0 & J_z \end{bmatrix} \begin{bmatrix} \omega_x \\ \omega_y \\ \omega_z \end{bmatrix} = \vec{\omega} \times J\vec{\omega} = \tilde{\omega} J \vec{\omega} \tag{46}$$

Next, the rotational motion will be related to the translational motion using relative motion principle. A beam with two hinges at the top and the bottom (A, B) and center of gravity (G) is shown in Figure 3-19.

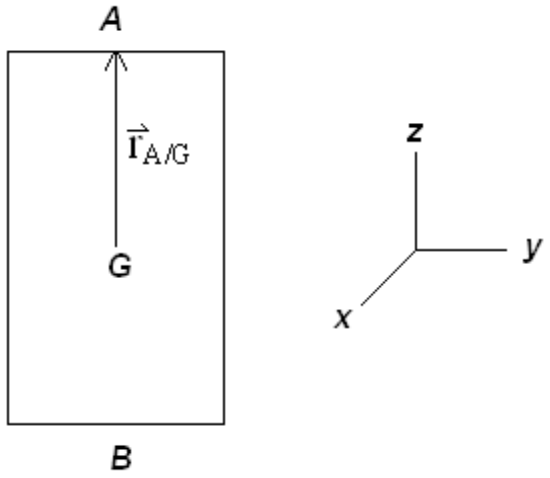

Figure 3-19 Front view of a beam with two hinges

Regarding the relative motion principle,

$$\vec{v}_A = \vec{v}_G + \vec{v}_{A/G} \tag{47}$$

$$\vec{v}_A = \vec{v}_G + \vec{\omega} \times \vec{r}_{A/G} = \tilde{r}_{A/G} \vec{\omega} \tag{48}$$

Where

$$\vec{r}_{A/G} = \begin{bmatrix} x \\ y \\ z \end{bmatrix} \tag{49}$$

$$\tilde{r}_{A/G} = \begin{bmatrix} 0 & z & -y \\ -z & 0 & x \\ y & -x & 0 \end{bmatrix} \tag{50}$$

Now, according to the mentioned theories, we can build the two hinges body submodel in 20-Sim (v.4.1, (2010) Controllab Products B.V., Enschede, Netherlands) as shown in Figure 3-20.

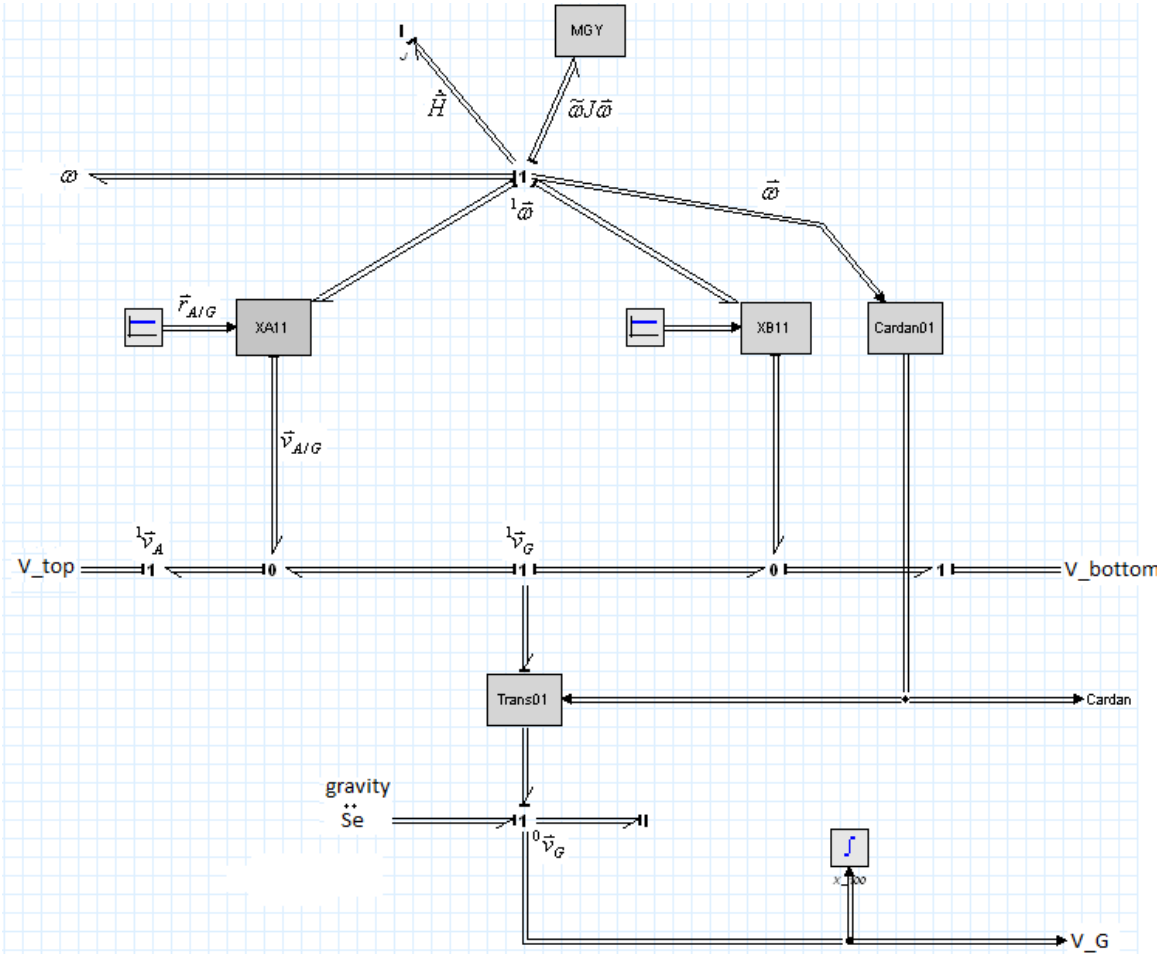

Figure 3-20 Bond graph model for a single body with two hinges

'1' indicates inertial coordinate and '0' indicates body-fixed frame

As can be seen in the Figure 3-20, the axial, lateral and torsional motion are coupled together in the single body. The 1-junction ($^1\vec{\omega}$) is responsible for the angular motion and the 1-junction ($^1\vec{v}$) is responsible for the axial and lateral motion in the body-

fixed frame. In the meanwhile, the 1-junction (${}^0\vec{v}$) gives the axial and lateral velocities in the inertial coordinate. An integrator has been used to attain the displacement of the center of gravity (CG) in three directions (one axial and two lateral) from corresponding velocities.

The I-element which is connected to the velocity of the CG (${}^0\vec{v}$) is the mass of the element. This is one of the advantages of the transformation from local coordinate to the global frame. If the mass was connected to the 1-junction of the body-fixed frame (${}^1\vec{v}$), we would need to transform the gravity direction of the element, but in the inertial coordinate the gravity is always in the Z direction. The effort source (Se) which is connected to the 1-junction of the CG (${}^0\vec{v}$) defines the gravity force.

Velocity of each hinge is obtained using relative motion principle, as mentioned before. Algebraic summation of the flows which are connected to the 0-junction should be zero, so $\vec{v}_A = \vec{v}_G + \vec{v}_{A/G}$. Finally the Cardan angles are calculated in Cardan01 block using equations (41)-(43). The equations of each block are shown in the appendix.

3.6. Continuous rod

Next, the single bodies should be connected together to make a rod with desired properties. To do so, we will use proper springs and dampers in the connection points of the bodies. In Figure 3-21, when the bottom hinge A of the body 1 is connected to the top hinge B of the body 2, the velocity of these two hinges should be equal, in presence of no axial deflection. We will use this assumption to have a continuous rod.

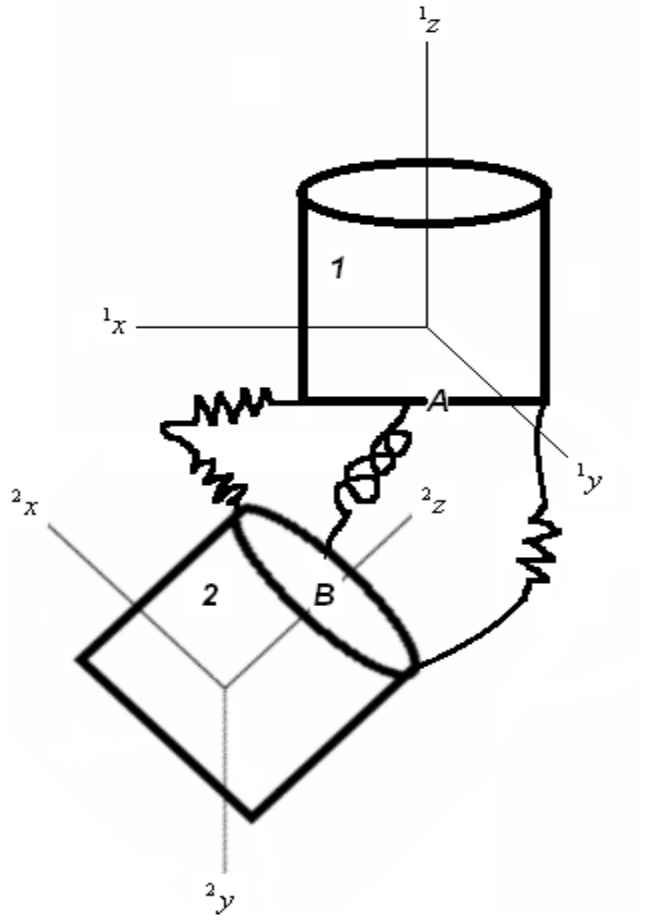

Figure 3-21 Connecting two bodies using $^1v_A = {}^2v_B$

In the bond graph model, those two hinges should be connected via parasitic elements that will be described afterward. Otherwise, we encounter derivative causality which is not desired. The parasitic element is a spring and a damper. As shown in Figure 3-22, first, the velocity of hinge (A) in the above figure is transformed to inertial coordinate. Then, this velocity is aligned to the velocity of the hinge (B). Finally, these two velocities is connected together using a parasitic element (R, C). This process will be repeated to add as many as elements we want.

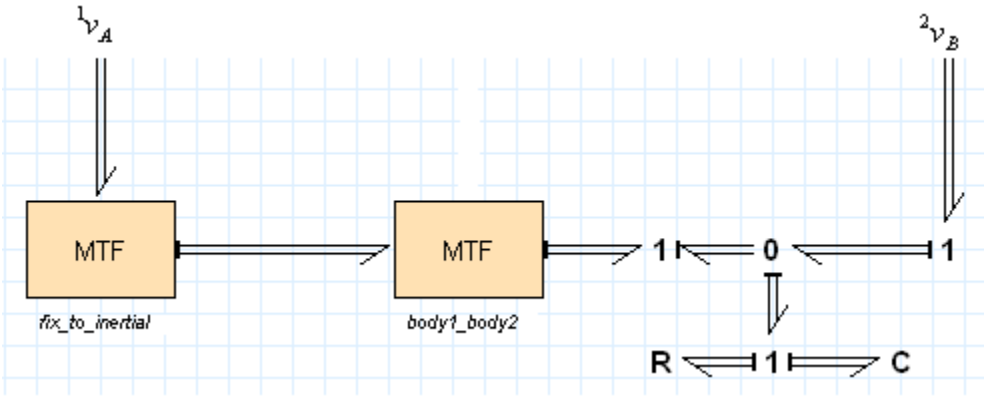

Figure 3-22 Connecting two elements in the translational motion (one axial and two laterals)

The equations of each block are shown in the appendix.

For the rotational motion, the same mentioned procedure for translational motion is repeated.

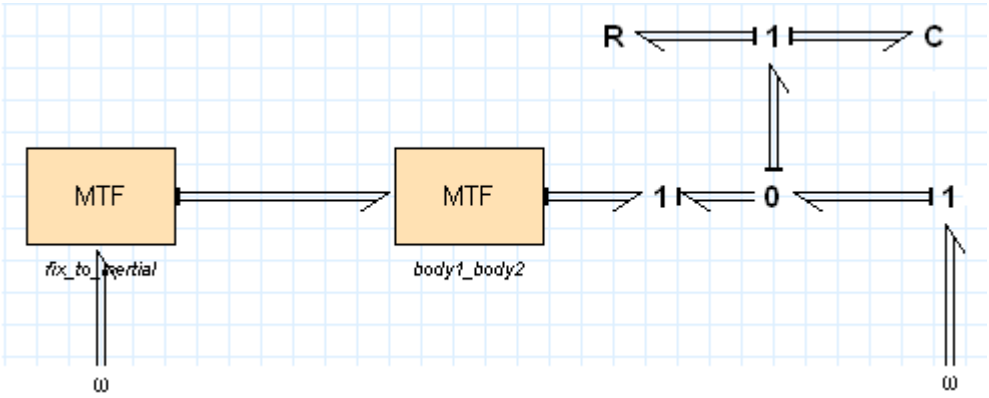

Figure 3-23 Connecting two elements in the angular motion (torsional)

Now, we are able to connect two elements in both translational and angular motions.

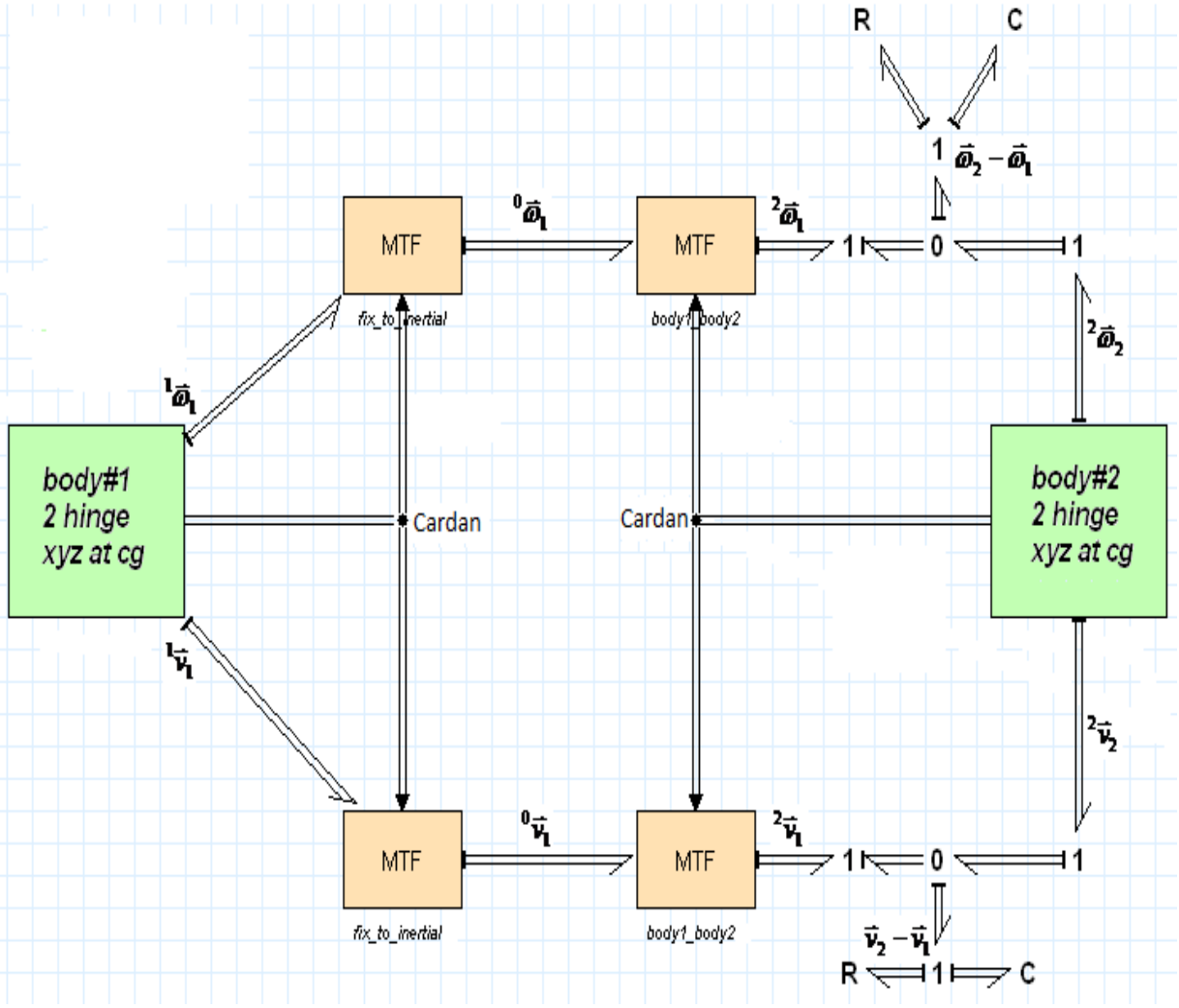

Figure 3-24 Two connected elements using parasitic elements

3.7. Parasitic Elements

As can be seen in Figure 3-25, there is a parasitic element in each motion direction between each two elements. The left hand side spring acts as a torsional spring and resists against torsional motion (ω). The middle spring is a linear spring and acts in axial modes (Z). The right hand side joint acts as a spherical joint and resists against lateral motions (X, Y).

To determine the stiffness of each spring we need 3×3 matrices for either translational or torsional motions. According to Ibrahim's (Ibrahim *et al.*, 1987) work on dynamics of a continuous beam, we can define the compliances in each direction:

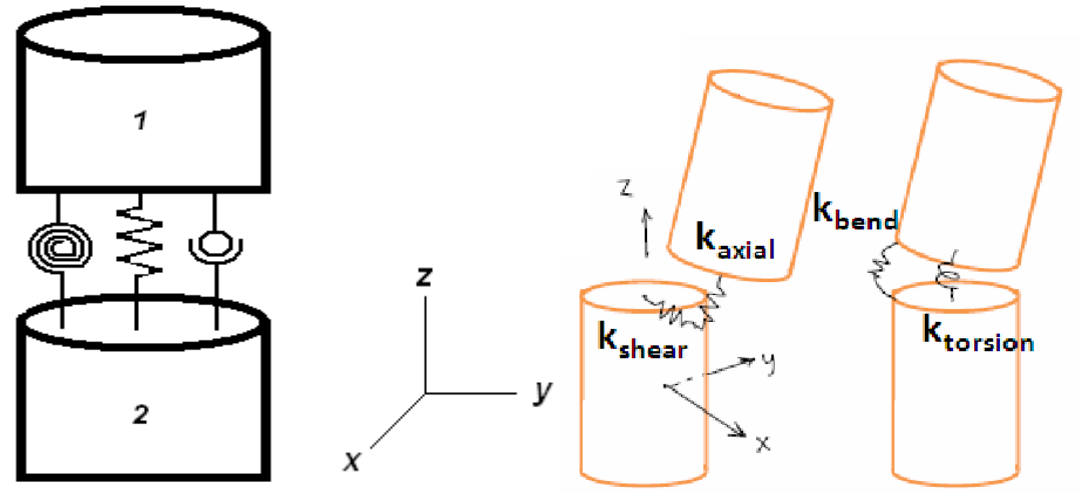

Figure 3-25 Parasitic elements between two bodies

$$C_{tran.} = \begin{bmatrix} C_{transverse} & 0 & 0 \\ 0 & C_{transverse} & 0 \\ 0 & 0 & C_{axial} \end{bmatrix} \tag{51}$$

$$C_{tors.} = \begin{bmatrix} C_{bending} & 0 & 0 \\ 0 & C_{bending} & 0 \\ 0 & 0 & C_{torsional} \end{bmatrix} \tag{52}$$

These are the compliances of the system. Compliance is the inverse of the stiffness in an elastic system, as stated below.

$$C_{transverse} = \frac{1}{K_{transverse}} = \frac{l}{xAG} \tag{53}$$

$$C_{axial} = \frac{1}{K_{axial}} = \frac{l}{EA} \tag{54}$$

$$C_{bending} = \frac{1}{K_{bending}} = \frac{l}{EI} \tag{55}$$

$$C_{torsional} = \frac{1}{K_{torsional}} = \frac{l}{GJ} \tag{56}$$

(Ibrahim *et al.*, 1987)

where l is the length of the element, A is the cross section area of the element, E is the modulus of elasticity, G is the shear modulus, I is the moment of inertia, J is the polar

moment of inertia, and *x* is the shear coefficient which for a cylindrical tube cross section is obtained from equation (57):

$$x = \frac{6(a^2 + b^2)^2(1+\upsilon)^2}{7a^4 + 34a^2b^2 + 7b^4 + \upsilon(12a^4 + 48a^2b^2 + 12b^4) + \upsilon^2(4a^4 + 16a^2b^2 + 4b^4)} \quad (57)$$

(Hutchinson, J. R., 2000)

where υ is the Poisson's ratio, *a* is outer radius and *b* is inner radius.

Along with the compliances between each two elements, there is a damper in each direction motion. Damping factors are defined using 3×3 matrices, similar to the compliances. For damping factors, there is no formula or equation, so they should be determined by experimental methods or adjusted by other numerical methods. In this research finite element method (FEM) is used to adjust the damping factors. Two exact same models are developed in 20-Sim and Abaqus (FEM software package) and several inputs are applied to the models. The inputs are in all three direction motions, separately, and they are modeled as impulses. Abaqus does not give the damping factors in matrix form, therefore the damping matrices in 20-Sim should be tweaked to reach the same response as Abaqus. At the end of the day, the constant damping matrices are obtained in such a way that the responses to the impulse inputs in both models are similar. The results are available in the next chapter.

In this project, only the collar section has been modeled because of the emphasis on the lateral vibration which mostly occurs in the drill collar because of its low natural frequency. As mentioned before, the lumped segment method has been used to simulate the drill collar. A 60 meters collar is modeled in 30 segments. Boundary conditions can be applied to any segment in any motion direction.

This model is easily expandable to more segments. One can add the other properties of the drillstring and real drilling conditions such as wellbore contact. In the next chapter, some case scenarios are considered and the results are interpreted.

The numerical values for one segment are shown in Table 2.

Table 2 Numerical values of the model

Length	60m	Density	7860kg/ m^3
Number of segments	30	Mass	414.84kg
Outer diameter	0.2m	Axial compliance	2770891200m/N
Inner diameter	0.08m	Transverse compliance	758925743.5m/N
Modulus of elasticity	210×10^9 Pa	Torsional compliance	6198879.5m/N
Poisson's ratio	0.3	Bending compliance	8035584.3m/N

4. Simulation Results

4.1. Validating results using Finite Element Method

The compliances between each two elements are defined and we need to adjust the damping factors, as well. For the damping factors there is no particular formula or relation. The only way to define the damping factors is adjusting with other methods, such as experimental or finite element method (FEM). Abaqus has been used to adjust the damping factors by comparing the results in FEM and 20-Sim. A model has been constructed in 20-Sim and the same model has been produced in Abaqus with the same properties and boundary conditions. The 60 meters fixed-free vertical collar section is constructed and impulse force is applied in all three dimensions, separately. In Abaqus we can apply damping ratio to the model. An arbitrary damping ratio of 10% has been applied to the beam in all directions because the drillstring structure should be under-damped. The same outcomes are reached after varying the damping matrices in 20-Sim.

For the axial motion, a fixed-free beam is considered. An impulse axial force at the free end (bottom) has been conducted. Figures (4-1)-(4-5) show the input, Abaqus output and resultant 20-Sim output after trial and error procedure.

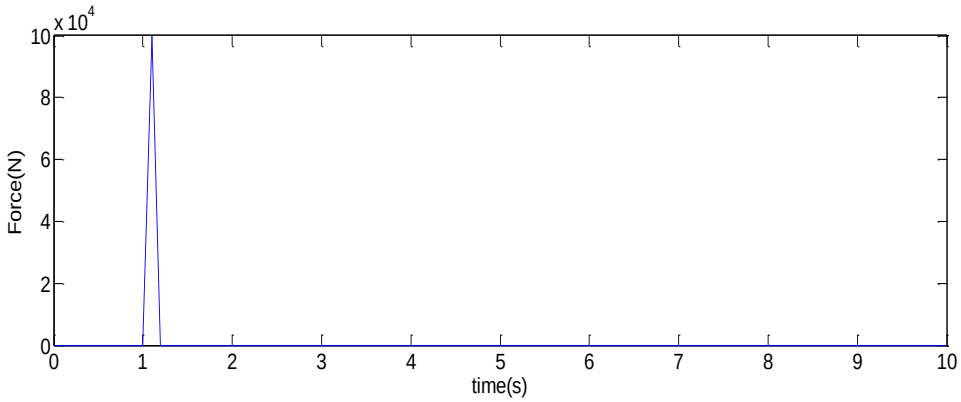

Figure 4-1 Axial Impulse force at the bottom of the collar section as an input

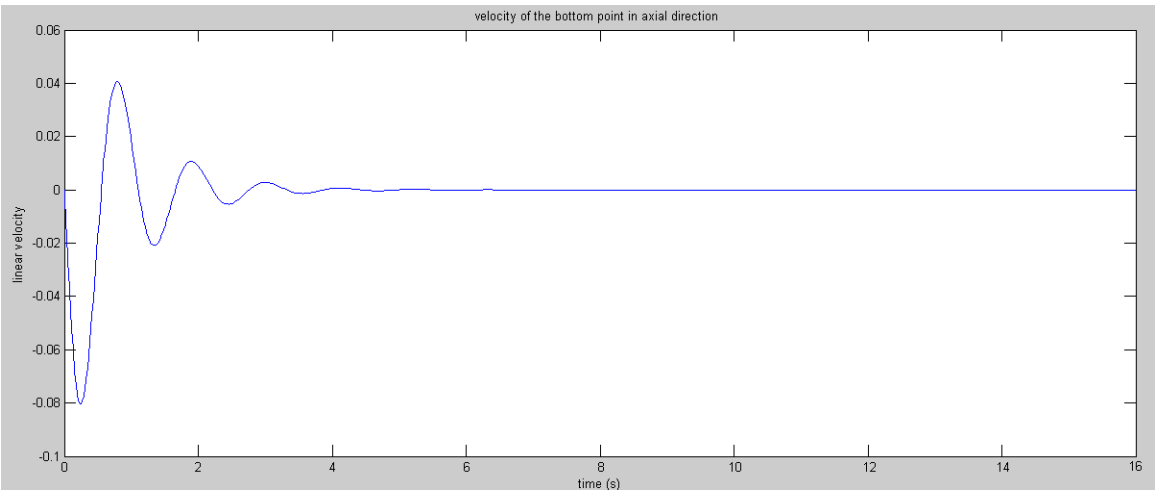

Figure 4-2 Linear axial velocity of the bottom point of the collar (20-Sim output)

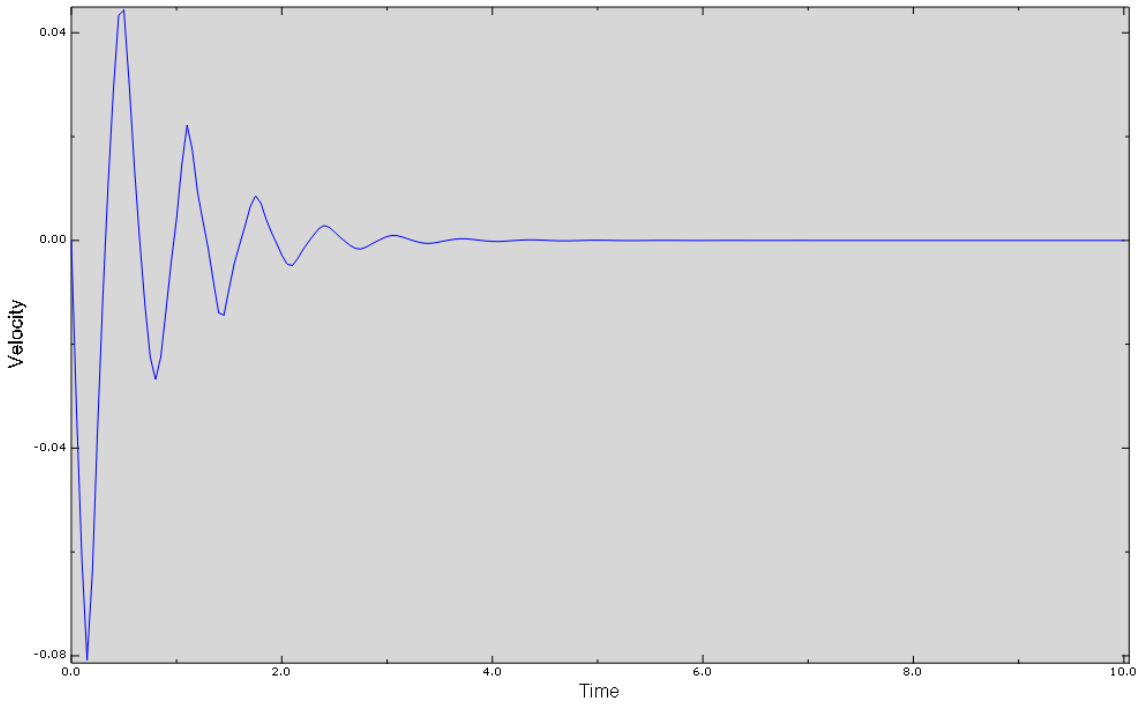

Figure 4-3 Linear axial velocity of the bottom point of the collar (Abaqus output)

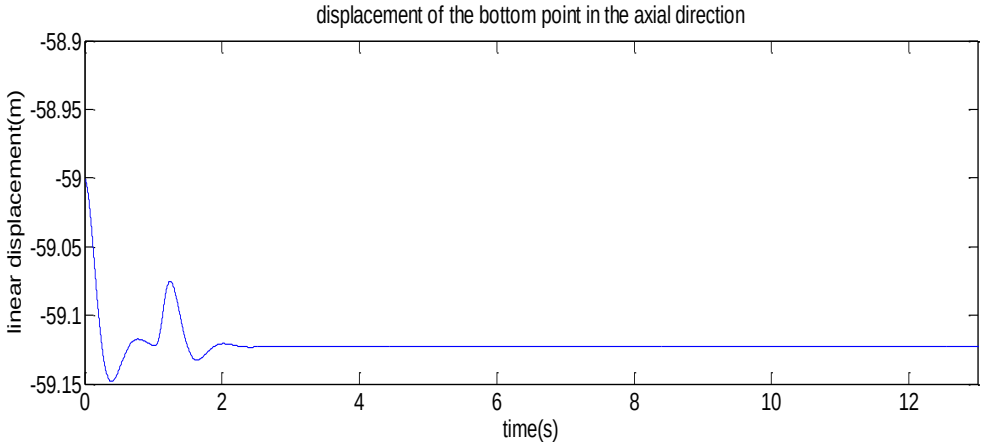

Figure 4-4 Linear axial displacement of the bottom point of the collar (20-Sim output)

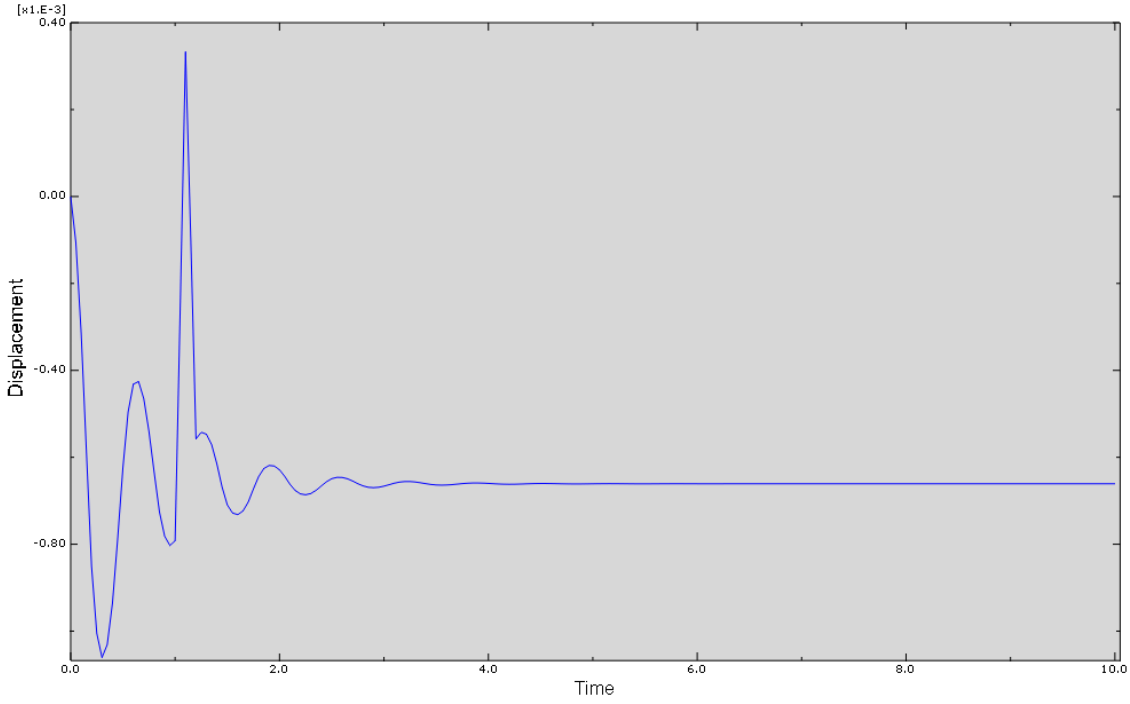

Figure 4-5 Linear axial displacement of the bottom point of the collar (Abaqus output)

For the torsional motion, the same fixed-free beam is used. Figures (4-6)-(4-10) show the input, Abaqus outputs and resultant 20-Sim outputs after trial and error procedure.

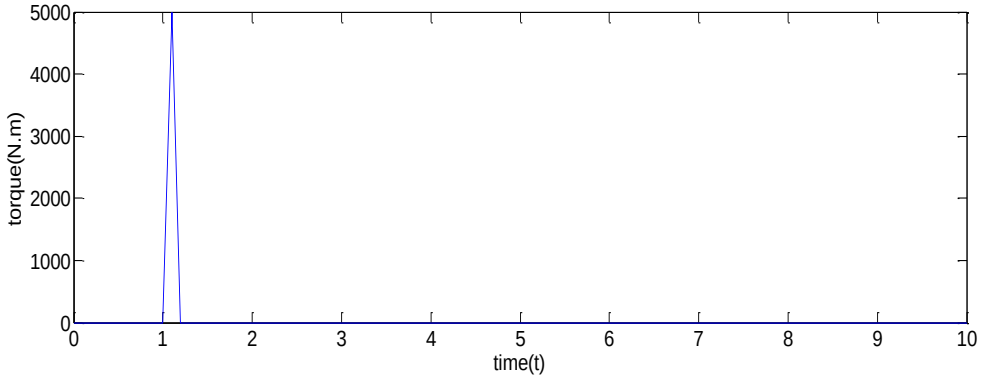

Figure 4-6 Torsional Impulse force at the bottom of the collar section as an input

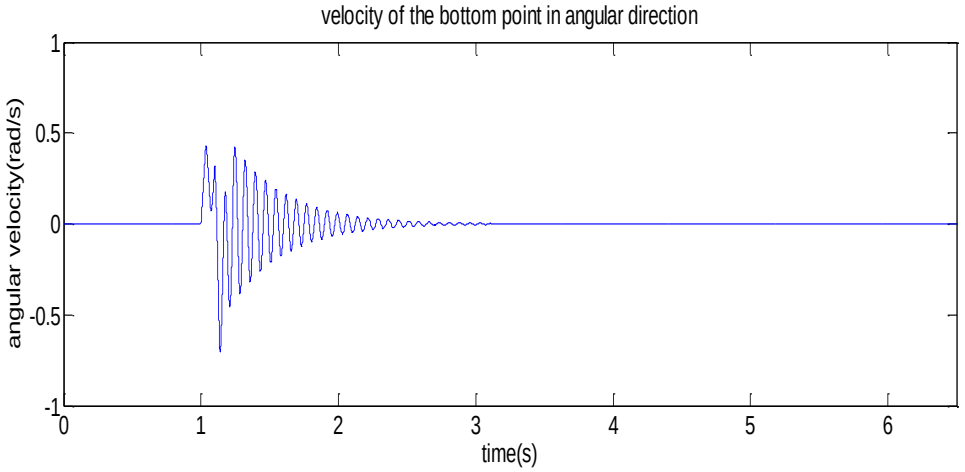

Figure 4-7 Angular velocity of the bottom point of the collar (20-Sim output)

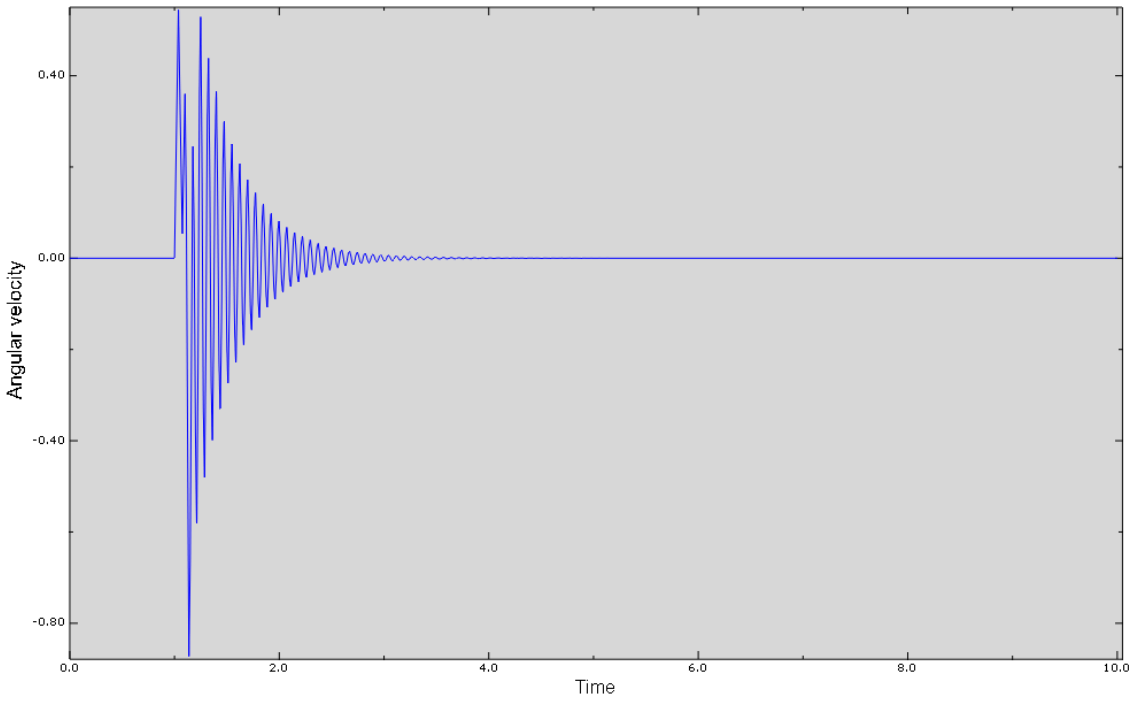

Figure 4-8 Angular velocity of the bottom point of the collar (Abaqus output)

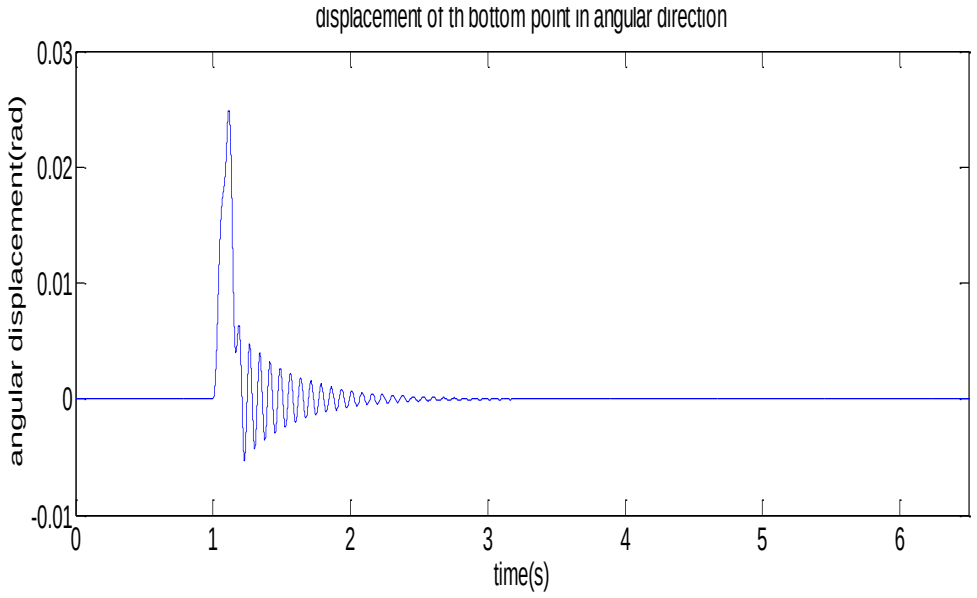

Figure 4-9 Angular displacement of the bottom point of the collar (20-Sim output)

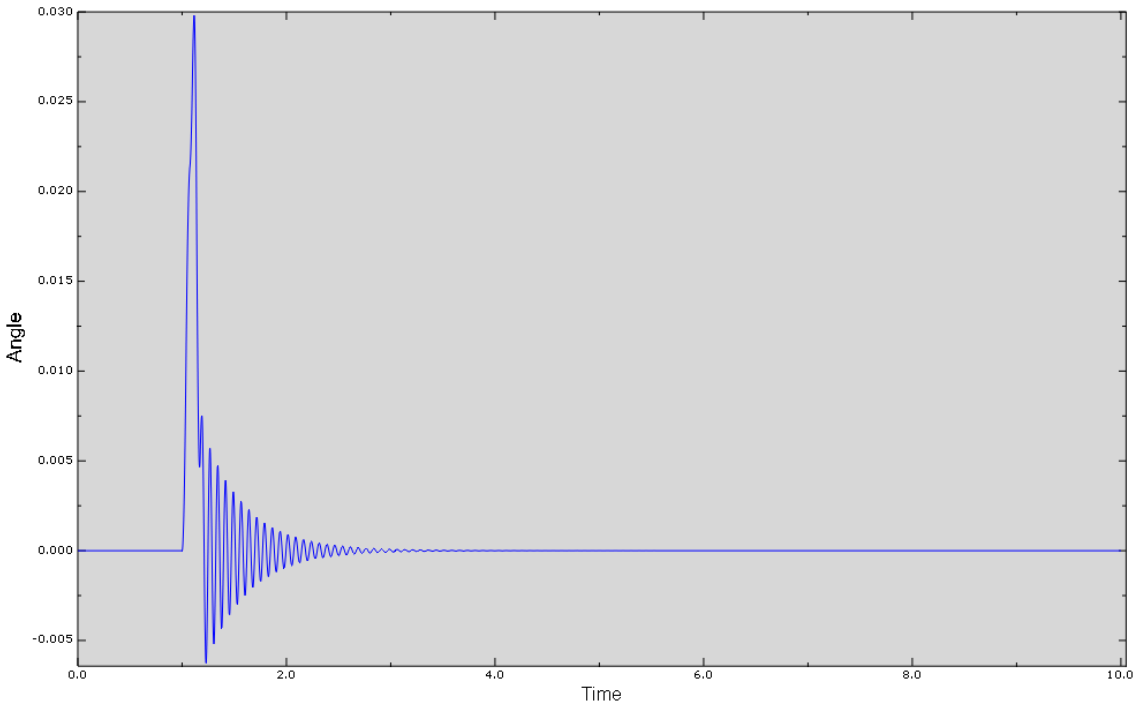

Figure 4-10 Angular velocity of the bottom point of the collar (Abaqus output)

4.2. Results

Up to now, we have focused on 60 meters collar section with adjusted damping factors, using FEM model. The 20-Sim model has 30 lumped elements and each element has two hinges. In the next step, we are trying to improve the model to include more realistic boundary conditions. To do so, 3-span collar will be constructed and hydraulic forces at the top and bottom of the collar due to mud effect will be added.

4.2.1. Angular velocity

First of all, we should examine the angular velocity and acceleration in the presence of constant torque at the top of the collar section. With no damping effect at the bottom (no bit-rock interaction) and constant torque at the top, the angular velocity of any point along the collar should remain the same when the torsional springs between elements are stiff. So, the model will act like a rigid body. Using Newton's law in the angular motion gives:

$$\sum T = I.\alpha$$

Where,

T = net external torque

I = moment of inertia

α = angular acceleration

The moment of inertia for 60 meters collar with cylindrical cross section (D_o = 0.2m; D_i = 0.08m) is 72.18 $kg.m^2$. Applied constant torque at the top is 5000 N.m. So, the angular acceleration (α) equals 69.27 rad/s^2. Figures 4-11 and 4-12 show the resultant angular velocity at the top and the bottom of the collar. The slope of these two should remain the same as discussed.

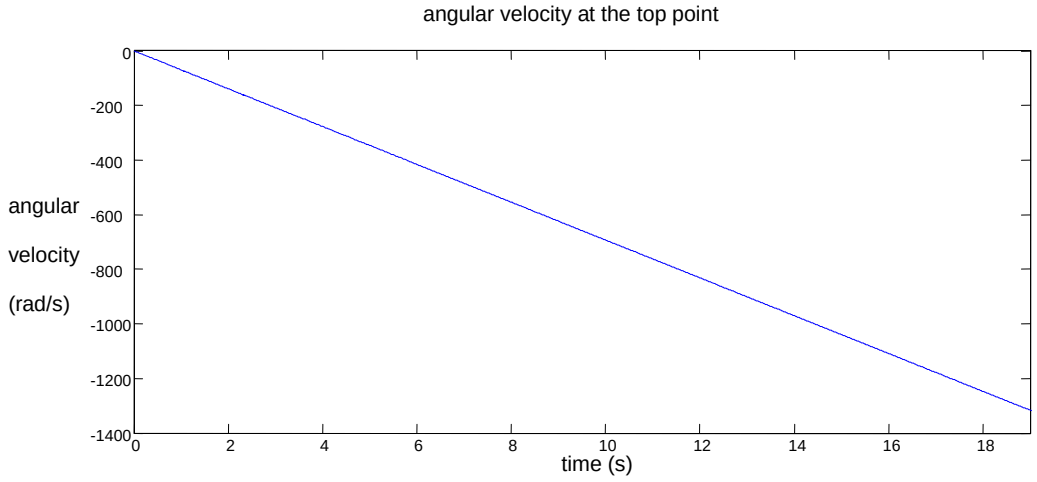

Figure 4-11 Angular velocity of the top point of the collar under the constant torque

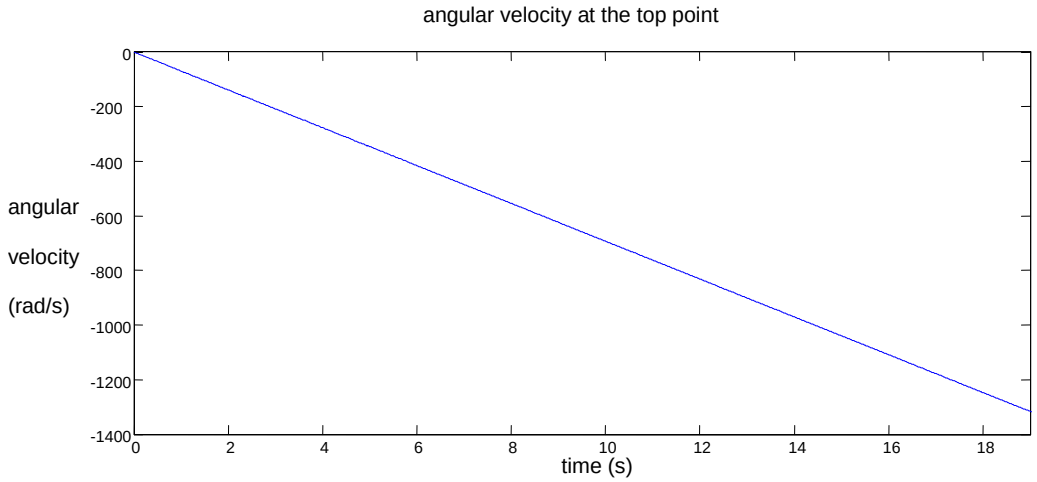

Figure 4-12 Angular velocity of the bottom point of the collar under the constant torque

As can be seen in above plots, the angular velocity along the collar remains the same. The slope of each figure shows the angular acceleration of the same point. The slope of these figures is exactly 69.27 rad/s^2. As a result, the model is in complete agreement with the theory.

4.2.2. Compression of the Collar Section

As mentioned before in literature, the pipe section should be in tension while the collar section should remain in compression in the drillstring due to the hydraulic forces. In Figure 4-13, the axial compliances in the collar in four different spots are illustrated. Positive value means compression and negative refers to tension. The compression load is increased with depth.

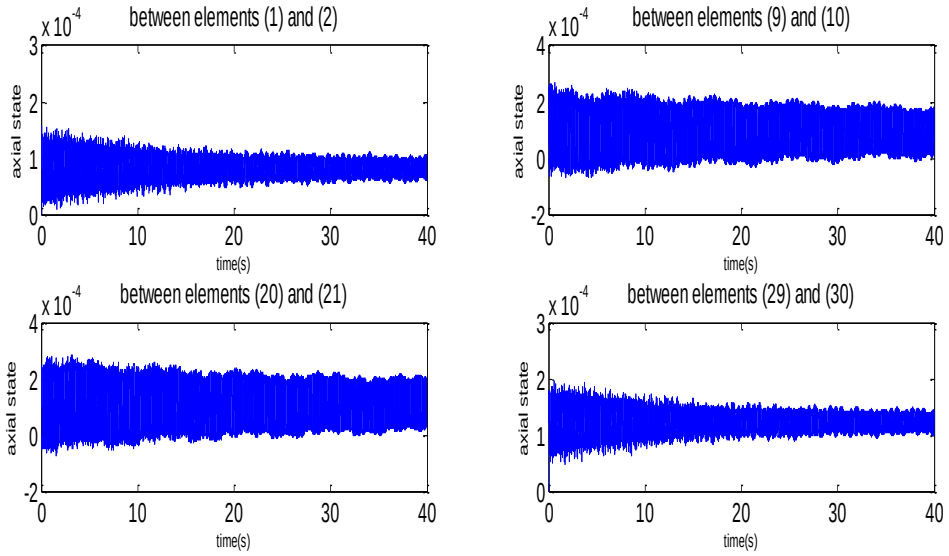

Figure 4-13 Axial compliances in four different spots of the drill collar in the presence of hydraulic forces (Positive values imply compression state)

4.2.3. Unbalanced Rotation

The center of gravity (CG) of each element is in the middle of the element in x, y and z axes. So, when the collar is rotating about the longitudinal axis, lateral deflection is not created. Moving the CG of the bit creates some lateral movement in two perpendicular directions with no lateral force. The displacement and velocity of such a lateral movement depend on how far CG is moved from the center and the stiffness of the stabilizers. Figure 4-14 shows the transverse displacement of the bottom of the collar, with no lateral force, by moving the CG of the bit from the center to 0.5cm far from the center.

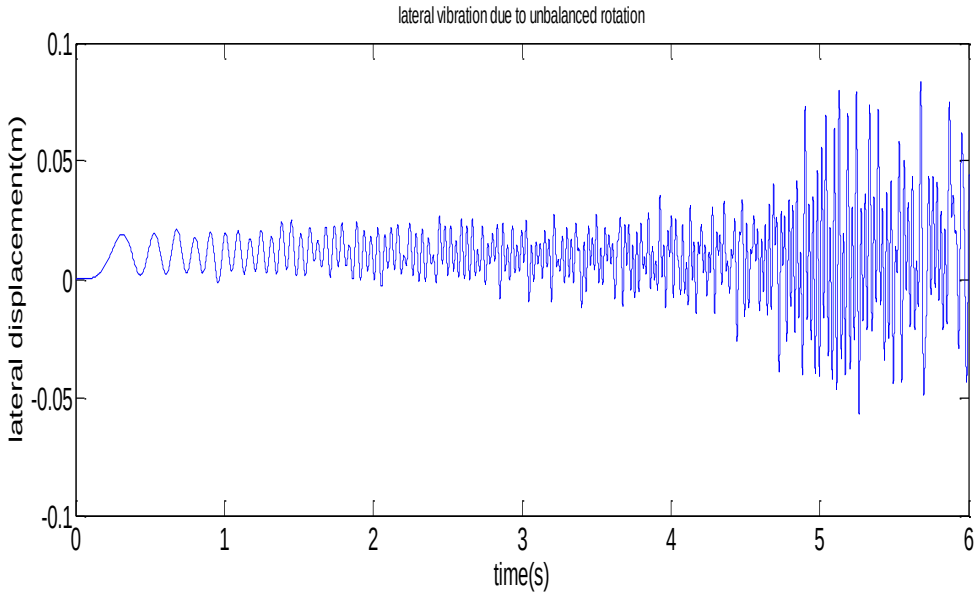

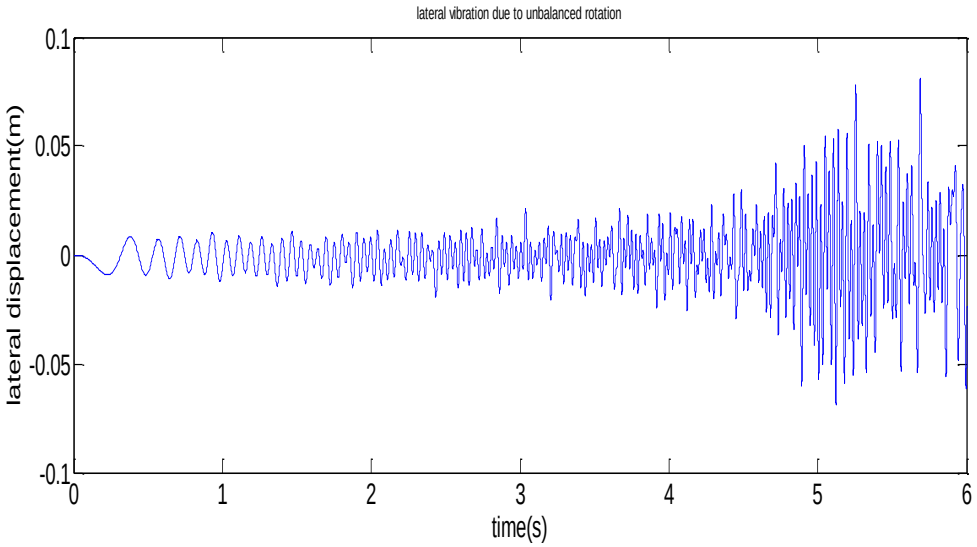

Figure 4-14 Displacement of the bottom point of the collar in two perpendicular lateral directions in unbalanced situation

As illustrated in above figures, the displacement of the bottom point of the collar has same behavior in two perpendicular directions (X, Y), but with different signs which was anticipated.

4.2.4. Vibration-Assisted Rotary Drilling (VARD) Tool

Any kind of vibration in the drillstring can affect the penetration rate as well as bit wear. In new drilling technology such as vibration-assisted rotary drilling (VARD), it is essential to study the effects of vibration on the drillstring. VARD tool applies the axial vibration to the drillstring which results in better ROP. Amplitude of the VARD tool can

reach as high as 20 percent of the applied WOB and frequency of 100 Hz is considered. The WOB is considered as 50kN, so the VARD force magnitude is 10kN.

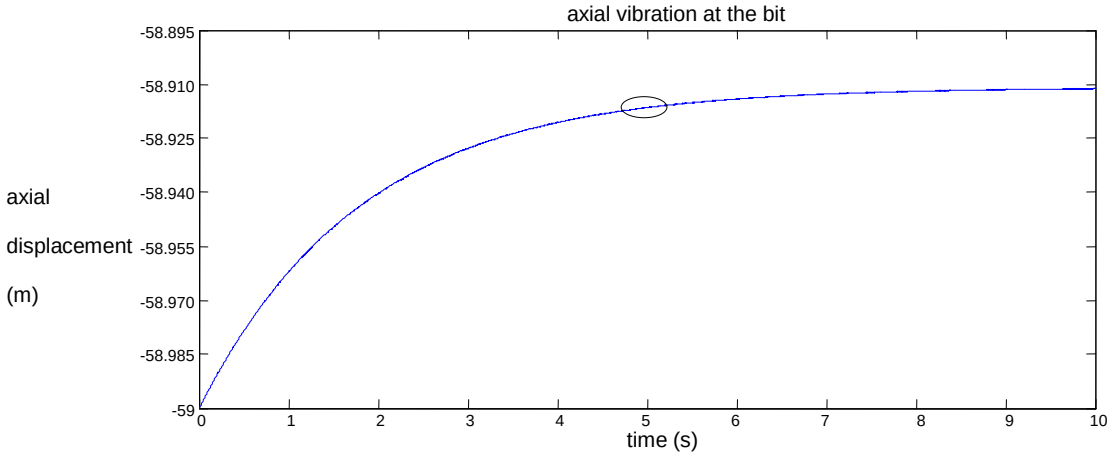

Figure 4-15 Axial displacement of the bit in presence of VARD tool

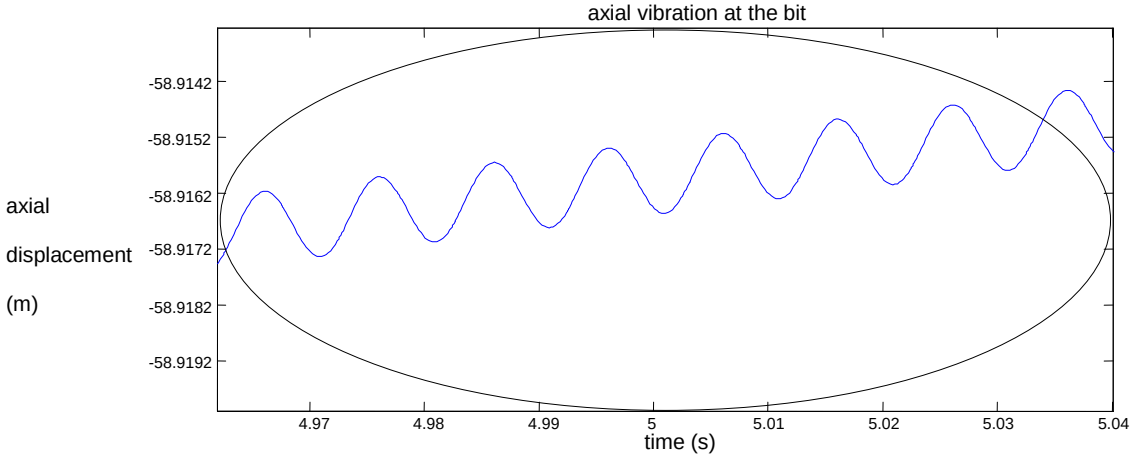

Figure 4-16 Zoomed in

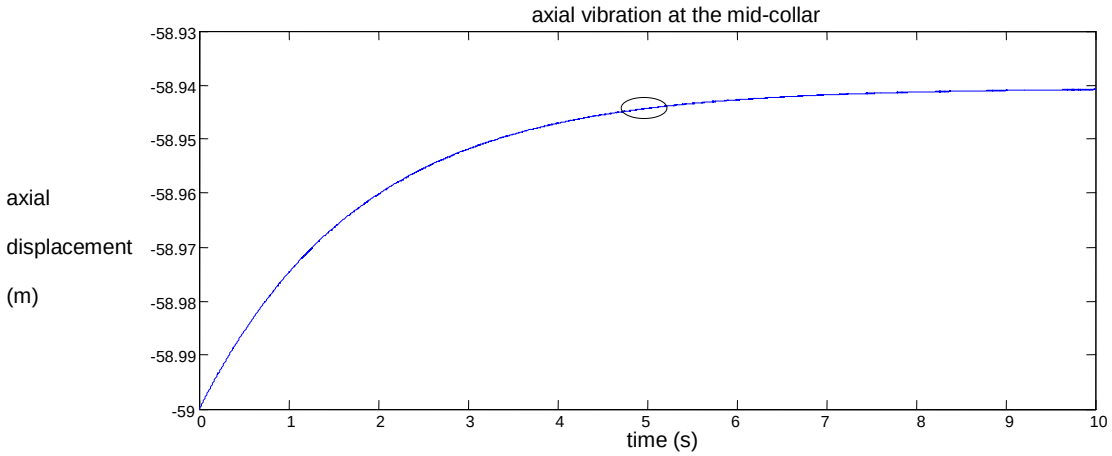

Figure 4-17 Axial displacement of the midpoint of the collar in presence of VARD tool

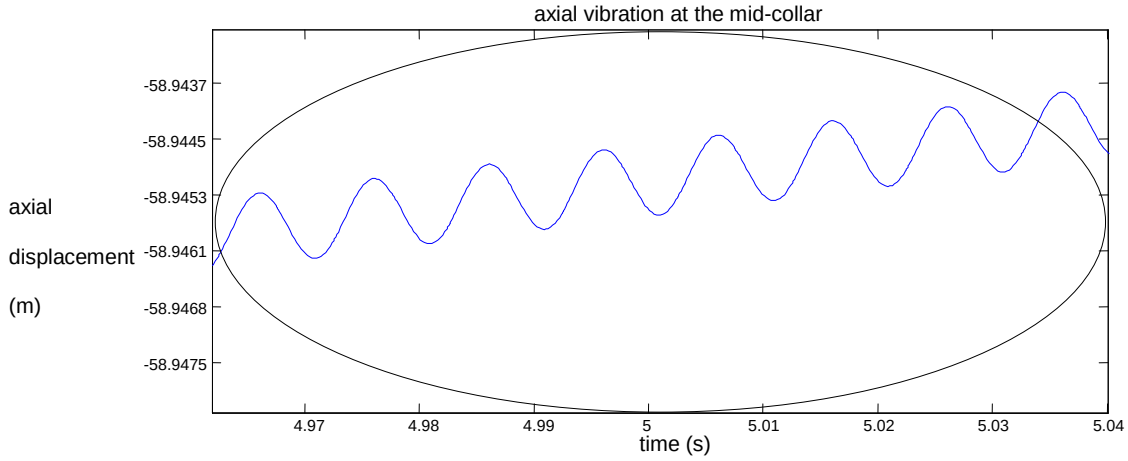

Figure 4-18 Zoomed in

The frequency of the VARD tool appears in the axial vibration in any point of the collar, as illustrated in above figures. The amplitude of the VARD tool is varying along the collar due to axial spring and dampers between each two elements. The VARD tool increases the bit-rock force that improves the ROP, but it causes unwanted axial vibration along the drillstring.

4.2.5. Natural frequency

If a system, after an initial disturbance, vibrates on its own, the frequency with which it oscillates without external forces is known as its natural frequency of vibration (Rao, J. S., 1992). Considering a spring, fixed at one end and having a mass attached to the other, the natural frequency of this single degree of freedom system depends on two system properties: mass and stiffness. The natural frequency (in radians per second) can be found from the following equation:

$$\omega_n = \sqrt{\frac{k}{m}}$$

where

k = stiffness of the spring

m = mass

ω_n = natural frequency (rad/sec)

Natural frequency of a beam is a function of the applied axial force. It has been shown that lateral natural frequency of a beam is higher when the beam is subjected to a tension force. Compression force reduces the natural frequency of the beam in lateral. In the 20-Sim model the collar section has been subjected to a compression force and a tension force, separately. A lateral impulse force has been applied at the middle of the collar to examine the relationship between natural frequency and applied axial force.

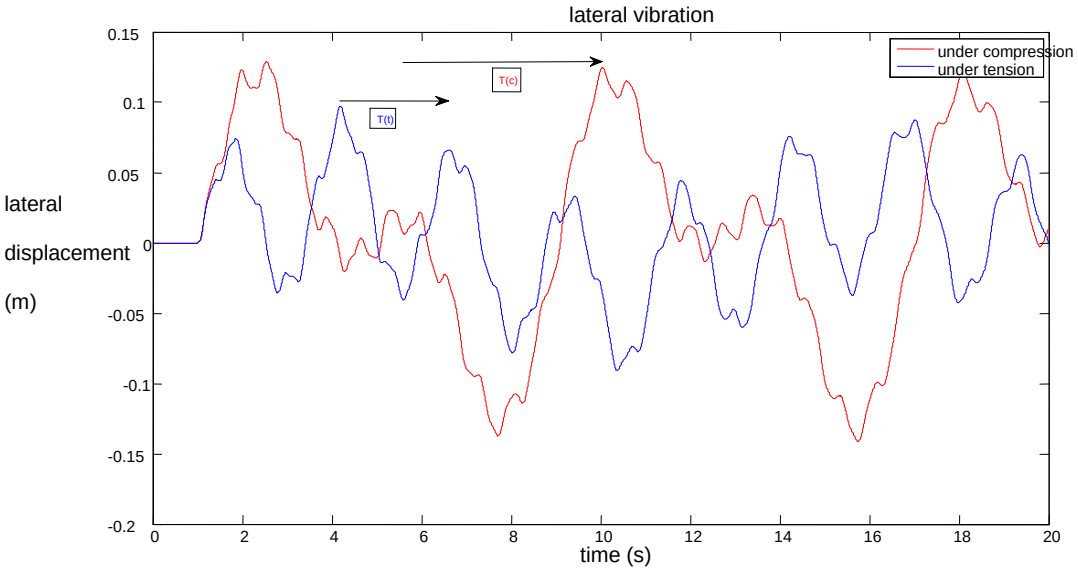

Figure 4-19 Comparison between natural frequencies

In the above figure, T(c) stands for peak to peak interval for the collar under compression and T(t) is the peak to peak interval of the collar while it is under tension. It is clear that the time interval between two peaks is higher when the collar is under compression. Therefore, the natural frequency of the beam is higher when it is under tension.

The natural frequency of a uniform simply supported beam subjected to an axial force *P* is calculated from (Rao, J. S., 1992):

$$\omega_n = \frac{\pi^2}{l^2}\sqrt{\frac{EI}{\rho A}\left(n^4 + \frac{n^2 P l^2}{\pi^2 EI}\right)}^{1/2}, \quad n = 0,1,2,...$$

Where l is the length of the element, A is the cross section area of the element, E is the modulus of elasticity, I is the moment of inertia, and P is the applied axial force (if the

axial force is compressive, $P<0$). Table 3 compares the natural frequency of a simply supported beam from the theory and the 20-Sim simulation.

Table 3 Natural frequency of a simply supported beam from theory and simulation

	Theoretical result		Simulation result	
	compression	tension	compression	tension
n=0	0	0	0	0
n=1	0.6710	0.8453	0.6911	0.8624
n=2	2.9646	3.1379	2.9823	3.1544
n=3	6.7809	6.9542	6.8019	6.9874
n=4	12.1230	12.2963	12.1612	12.3419
n=5	18.9913	19.1645	19.1325	19.2043
n=6	27.3857	27.5589	27.4139	27.6026
n=7	37.3063	37.4795	37.3581	37.5106

As a result, the model is in agreement with theory in frequency domain point of view.

4.2.6. Lateral vibration

As previewed in the literature review, the most destructive vibration in the drillstring is lateral vibration. Moreover, lateral vibration mostly occurs in the BHA section of the drillstring due to the low natural frequency of the collar with respect to the drill pipe.

Stabilizers are used in the BHA to prevent lateral vibrations. In the 20-Sim model, the 3-span collar has been simulated. To model the stabilizers, a stiff spring and damper has been considered which prevents any displacement in lateral directions, but has no effect on axial and torsional motions.

Lateral vibration can happen due to two main reasons. First, any lateral force will result in transverse displacement and resultant vibration. Secondly, as shown before, unbalanced rotation causes lateral motion. Figure 4-18 shows the 3-span BHA that has been simulated in 20-Sim.

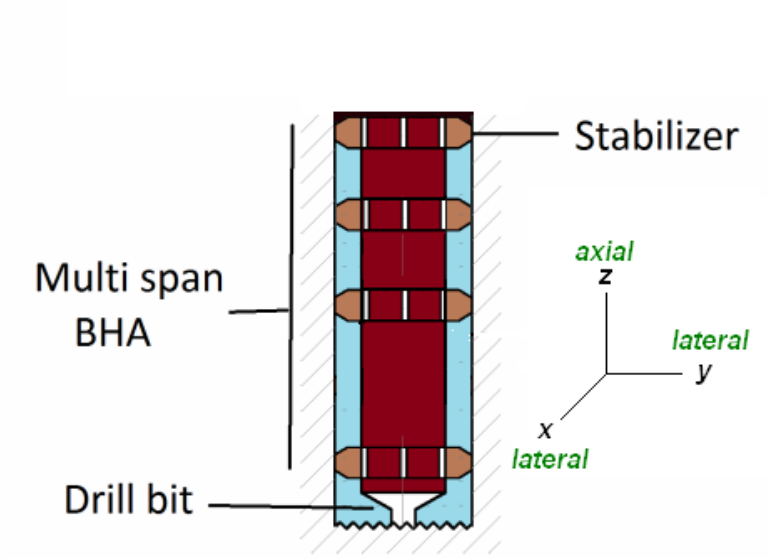

Figure 4-20 Multi span BHA

For the first scenario, an impulse force with amplitude of 2000N at the middle of the collar has been applied. Lateral vibration of three points of the collar is shown in Figure 4-19; at the middle of the collar, at the middle of the third span, and at the bit.

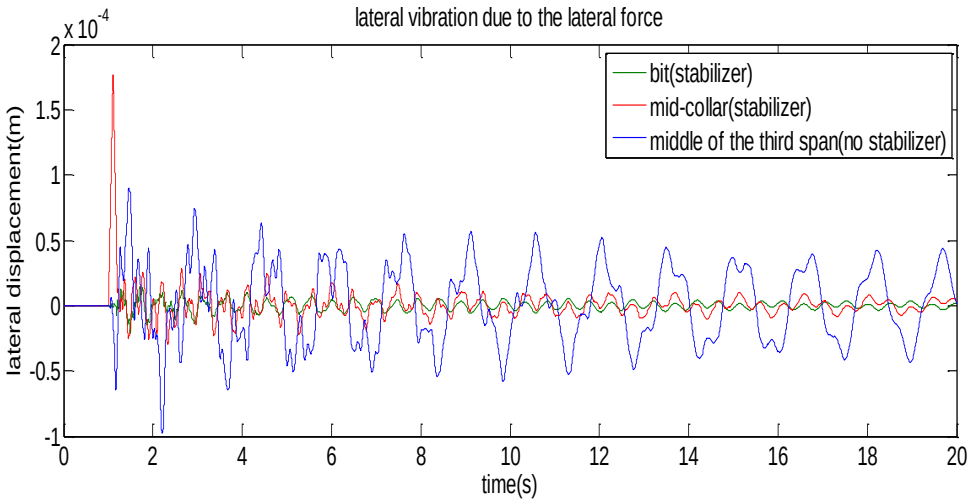

Figure 4-21 Lateral vibration due to the lateral force in three different locations

In the second simulation, COG is moved from the center to create lateral vibration. In this case there is no lateral force.

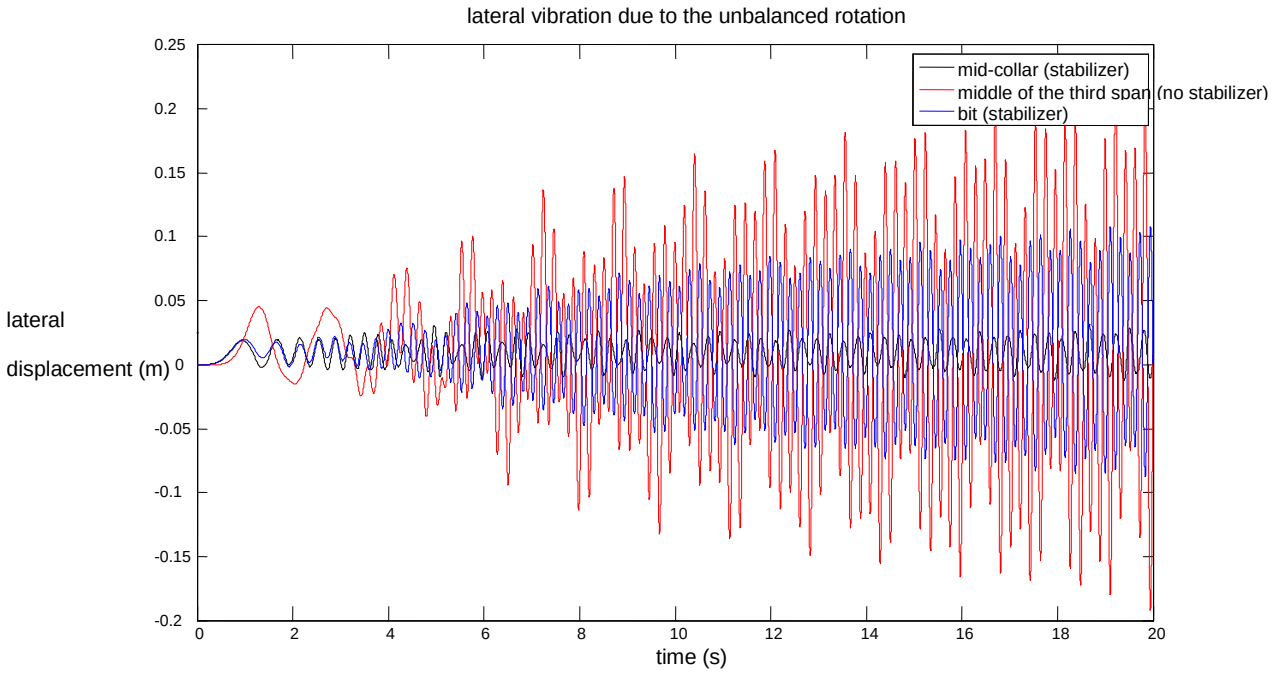

Figure 4-22 Lateral vibration due to unbalanced rotation in three different locations

In both cases, lateral vibration is relatively controlled at the bit and middle of the collar because of the presence of stabilizers, but above the bit more severe vibration occurs.

4.2.7. Coupled mode vibration

As mentioned before, the great advantage of this work is to simulate three coupled vibration modes. In previous sections, each single vibration mode was simulated and interpreted. The scope of this section is to show all three modes simultaneously.

The same 3-span collar section has been considered. Also, hydraulic forces at the top and the bottom of the collar have been applied due to the mud circulation effect. Previously, the lateral vibration of the collar due to the unbalanced rotation was shown. Here, the displacement of the axial and torsional springs between two random elements (elements 20 and 21) is illustrated in presence of hydraulic forces.

The hydraulic forces are calculated from:

$$F_{top} = \rho_{mud} g l_{pipe} \left(A_{collar} - A_{pipe} \right)$$

$$F_{bottom} = \rho_{mud} g \left(l_{pipe} + l_{collar} \right) A_{collar}$$

where ρ_{mud}=1500kg/m^3, l_{pipe}=700m

for aforementioned collar properties:

F_{top} = 223284N

F_{bottom}= 295224N

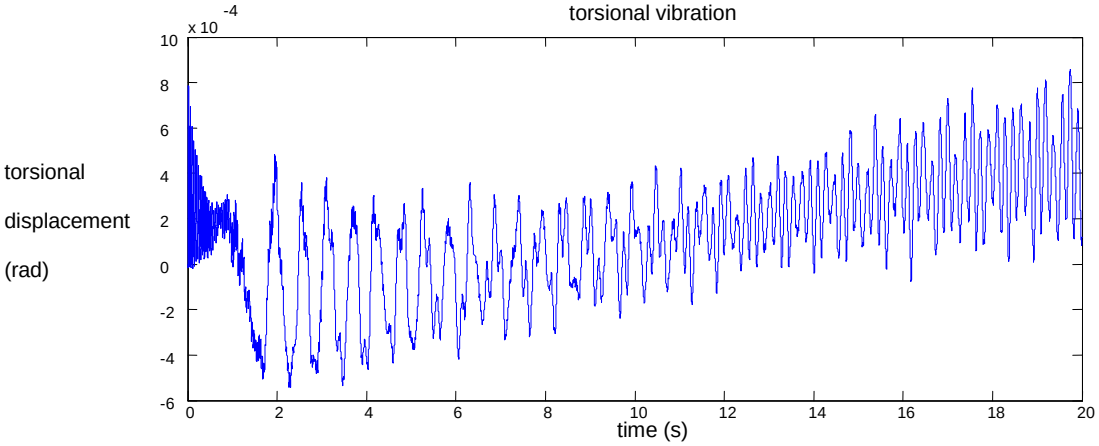
torsional vibration
x 10 -4
torsional
displacement
(rad)
time (s)

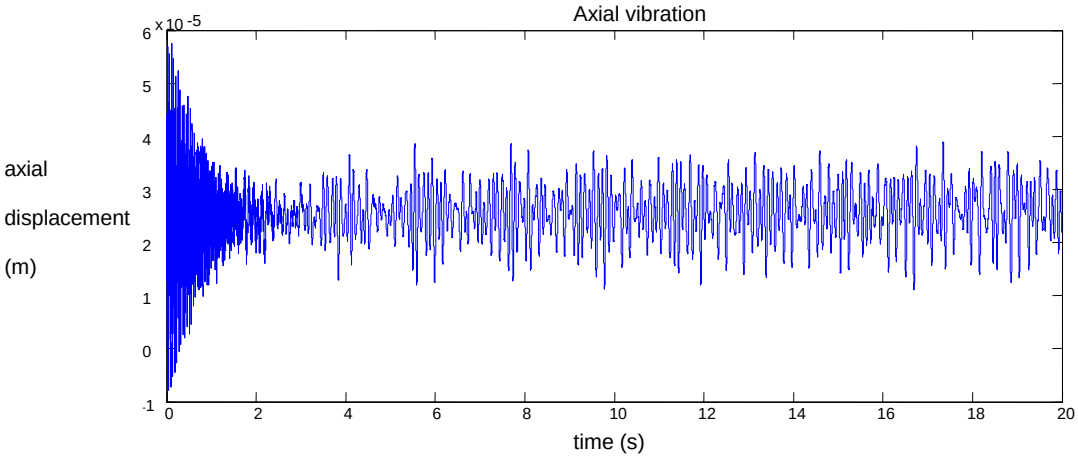
Axial vibration
x 10 -5
axial
displacement
(m)
time (s)

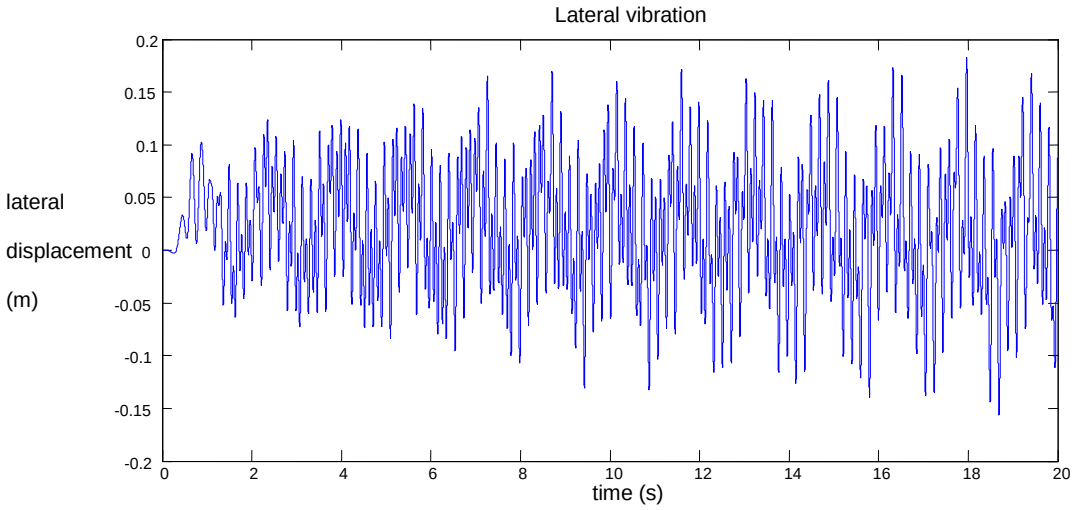

Figure 4-23 Coupled axial-torsional-lateral vibration due to unbalanced rotation

Figure 4-21 shows the axial, torsional and lateral vibration at the middle of the third span, respectively. The collar is in compression and all three modes have been shown.

In addition, the lateral displacement at the bit has been plotted. Figure 4-22 clarifies the importance of the stabilizer which causes less lateral vibration at the bit.

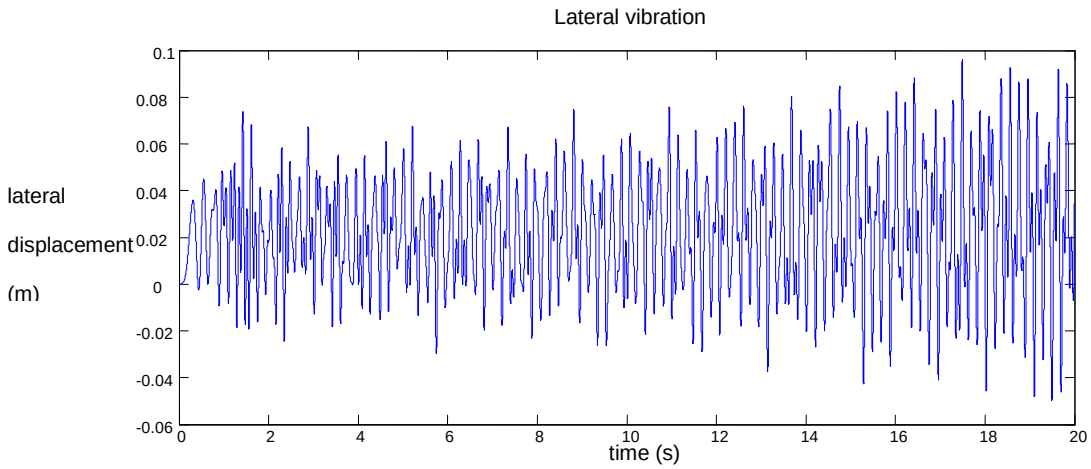

Figure 4-24 Reduction in lateral vibration in presence of the stabilizer

4.2.8. Rock-bit interaction

In the previous simulations, the bit was freely rotating without any resistance. Researchers have tried to simulate the rock-bit interaction in different ways. Applying sinusoidal force or displacement at the bit, considering a torsional damper at the bit, and implementing a reverse torque which resists the rotary table rotation are three examples of modeling the bit-rock interaction.

In this work, a resistant torque at the bit has been considered. Assuming a tri-cone bit, a torque with the frequency of three times of the rotation angle of the bit has been applied. In this case, self weight of the drillstring and hydraulic forces cause axial vibration and unbalances rotation results in lateral motion. Moreover, the resistant torque at the bit builds torsional vibration in the collar. Figure 4-23 illustrates the axial, lateral and torsional vibrations of the middle of the last span which is above the bit.

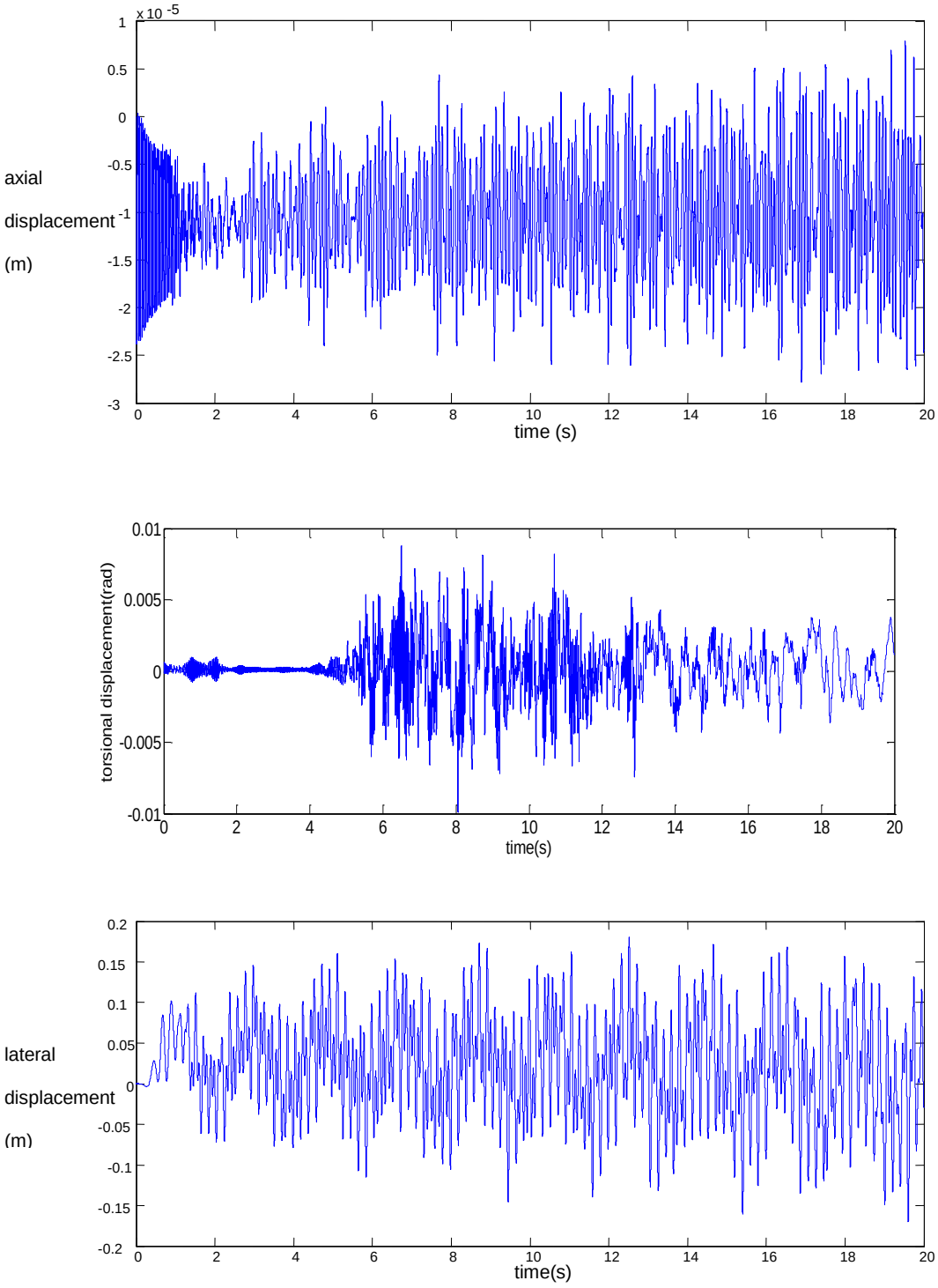

Figure 4-25 Coupled axial-torsional-lateral vibration due to the rock-bit interaction

It was shown before that without any damping at the bit and a constant rotary speed at the bottom, angular velocity of each point along the collar remains nearly the same. Implementing rock-bit interaction causes difference between rotary speeds of any two points. Torsional vibration which is shown in Figure 4-23 is the main reason of rotary speed difference. Figure 4-24 shows the drag torque at the bit and in Figure 4-25 the angular velocity of three points in the collar is shown.

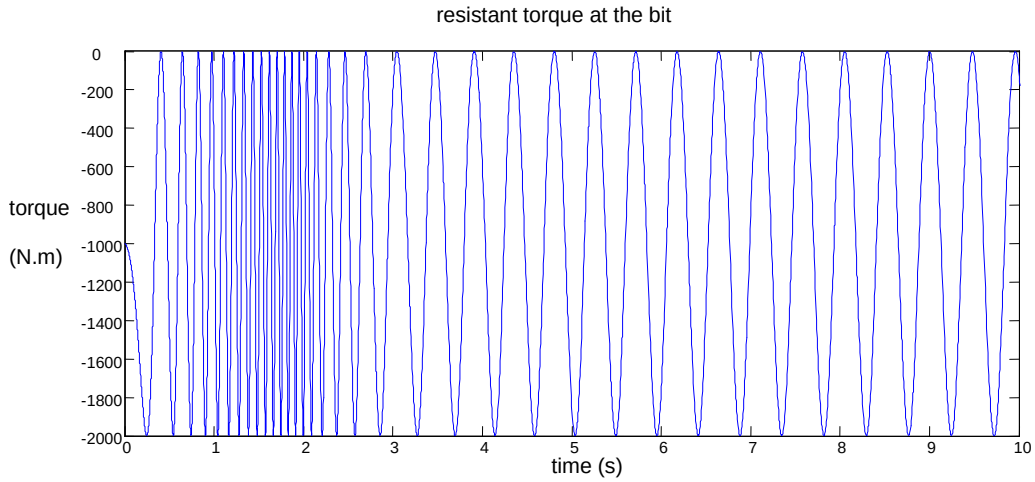

Figure 4-26 drag toque at the bit due to bit-rock interaction

This reaction torque is applied two seconds after rotating the drillstring. This is the reason that the angular velocity in the next figure is slowing down after two seconds.

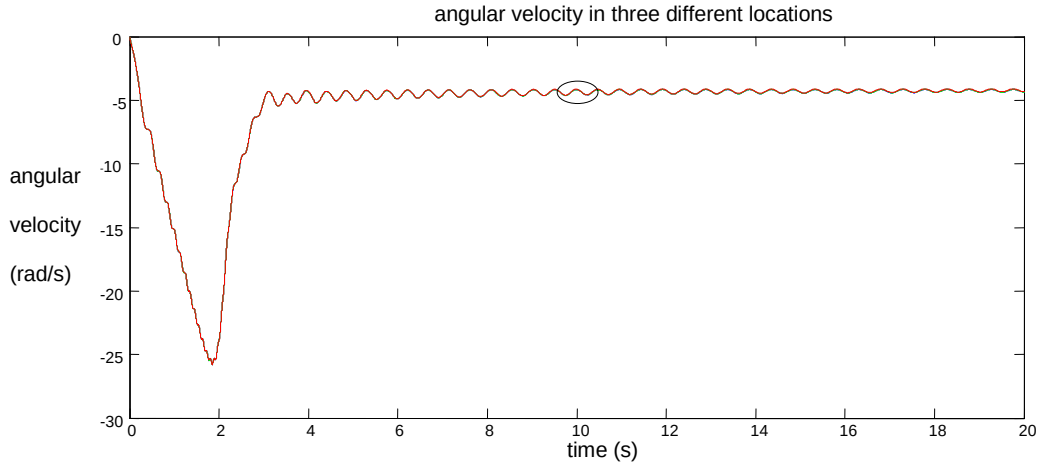

Figure 4-27 Angular velocity in three different locations

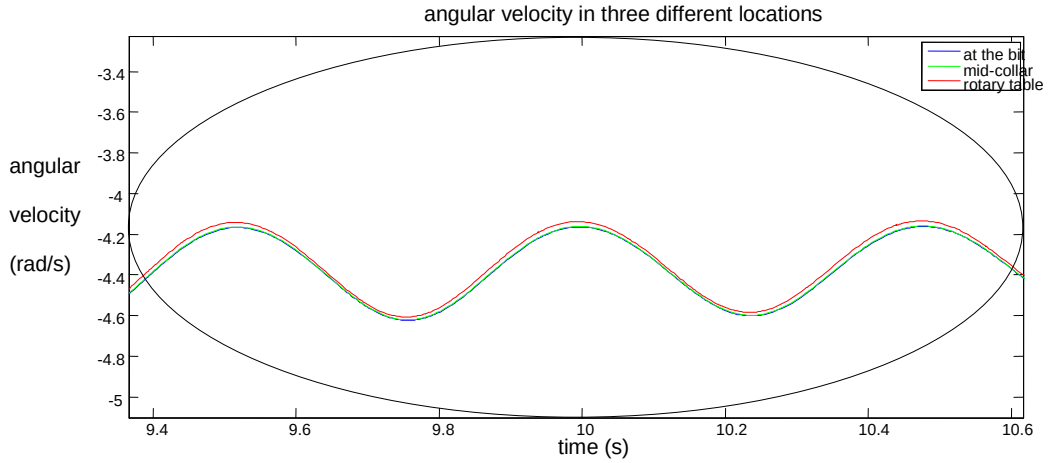

Figure 4-28 Zoomed in

According to above figures, the angular velocity is increased at the beginning and when the rotary torque at the top senses the drag torque at the bottom, the angular velocity is decreased and becomes steady. Moreover, the difference between the angular velocities is illustrated which occurs because of the torsional vibration due to the drag torque.

5. Concluding remarks and future work

This study presented an overview on vibration behavior of a drillstring with an emphasis on the coupled axial-lateral-torsional vibration and also including the effect of axial vibration on the drillstring. ADG has been seeking new technologies to improve the ROP and enhance drilling operation and also reduce drilling failure.

The main focus in this study is on the investigation of the coupled axial-lateral-torsional vibration behavior of the drillstring. Several methods were detailed and lumped segment method was selected for further analysis. Euler's equations were written in three dimensions which are derived from basic second Newton's law. Bond graph modeling was used for the computer simulation analysis and the basic of bond graph was detailed in chapter 3. The generated equations were then used in a 20-Sim model to predict the vibration behavior of the drillstring in 3-D direction.

After constructing lumped segments, they need to be connected via parasitic elements. Parasitic elements are made of springs and dampers in all three directions. Spring stiffness is calculated from some given equations, but for the damping factors an FEM model is used, so the damping factors are adjusted in three directions. The model is easily expandable to more segments and different drillstring features. Fast running time is one of the advantages of the bond graph modeling. Despite the fact that lumped segment modeling is not accurate in comparison with FEM model, this research shows the strong potential of the bond graph model in 3-D.

Results confirm that in the presence of the constant torque and without any resistant, the angular velocity of the whole beam remains the same. Moreover, moving the center of gravity of the bit with the constant rotary torque will result in transverse vibration along the beam. Resultant lateral vibration strongly depends on the distance of the COG from the center of the section. On the other hand, implementing bit-rock interaction will result in difference between the angular velocity along the collar. It occurs because of the torsional vibration which is the rock-bit interaction consequence.

VARD tool implementation on the collar causes the instantaneous frequency along the collar. Conducted simulation shows that amplitude of such a vibration depends on the damping ratio of the collar. The amplitude has the more value at the VARD tool and less value far from the VARD tool.

In addition it has been shown that stabilizers have great effect on reducing the lateral vibration. Lateral vibration which happens due to either the unbalanced rotation or the lateral force is reduced dramatically in the presence of the stabilizers.

Finally, the strength of the model has been showed in capturing all vibration modes, simultaneously.

In this research, only collar section was modeled because of the importance of the collar section in the frequency domain of the drillstring, so complete drillstring is one of the remaining tasks for the future work. However in the current model, the properties of the pipe section and corresponding equations have been generated and one needs to add additional elements in the model, simply.

In the future work, wellbore contact can be added to the model. The wellbore can be modeled as a very stiff spring, so the lateral movements cannot exceed the wellbore radius, and if any point contacts the wellbore, the model can predict the contact point. Bit-rock interaction in torsional was simulated, but the interaction in axial remains for further study. Friction is one of the important effects which has a great effect on frequency response and time response. Study of the friction effect on the response was beyond of the scope of this work, but resultant friction due to the mud circulation in axial, lateral and torsional directions can be extracted and implemented into the model.

Determining realistic parameters is needed for more accurate and realistic simulation. In this regard, collaboration with industry partners can be helpful. Validation with laboratory experiments is also a strong way to prove the simulation results. Moreover, it has been revealed that adding a shock sub can reduce the axial vibration of the drillstring. Basically, adding a damper and a spring to the one of the spans in the collar will simulate the shock sub.

References

ABAQUS Theory Manual (version 6.10), 2012, Dassault Systèmes Simulia Corp., RI, USA

Abbasian, F. et al. (1998). *Application of stability approach to torsional and lateral bit dynamics.* SPE Drilling and Completion conference, Texas, USA.

Ashley, D. K. et al. (2001). *Extending BHA life with multi vibration measurements*. IADC/SPE Drilling conference, Texas, USA.

Bailey, J. R. et al. (2008). *Development and application of BHA vibrations model*. International Petroleum Technology conference (IPTC), Malaysia.

Berlioz, A. et al. (1996). Dynamic behavior of a drillstring: Experimental investigation of lateral instabilities. *Journal of Vibration and Acoustics*, vol. 118, 292-298.

Challamel, N. et al. (2000). *A stick-slip analysis based on rock-bit interaction: theoretical and experimental contribution*. IADC/SPE Drilling conference, U.S.A.

Chen, S. L. (1995). An improved transfer matrix technique as applied to BHA lateral vibration analysis. *Journal of Sound and Vibration*, vol. 185 (1), 93-106.

Chen, S. L. et al. (1999). *Field investigation of the effects of stick-slip, lateral and whirl vibration on roller cone bit performance*. SPE Annual conference, Texas, USA.

Chien-Min Liao (2011). *Experimental and numerical studies of drill-string dynamics.* Unpublished Dissertation. University of Maryland, College Park.

Chin, W. C. (1994). *Wave propagation in petroleum engineering*. Texas: Gulf Publishing Company.

Christoforou, A. P. (1997). Dynamic modeling of rotating drillstrings with borehole interactions. *Journal of Sound and Vibration*, vol. 206 (2), 243-260.

Christoforou, A. P. et al. (2001). *Active control of stick-slip vibrations: The role of fully coupled dynamics*. SPE Middle East Oil Show, Bahrain.

Dareing, D. W. et al. (1968). Longitudinal and angular drillstring vibrations with damping. *Journal of Engineering for Industry, Transaction of the ASME,* vol. 90, No.1, 54-61.

Elsayed, M. A. et al. (1997). Effect of downhole assembly and polycrystalline diamond compact (PDC) bit geometry on stability of drillstrings. *Journal of Energy Resources Technology*, vol. 119, 159-163.

Elsayed, M. A. et al. (2002). *Analysis of coupling between axial and Torsional vibration in a compliant model of a drillstring equipped with a PDC bit*. ASME Engineering Technology conference on Energy (ETCE), U.S.A.

Gabriel, P. G. et al. (1997). *Drillstring vibration: How to identify and suppress*. 5th Latin American and Caribbean Petroleum Engineering conference, Rio de Janerio, Brazil.

Ghasemloonia, A. et al. (2012). Vibration analysis of a drillstring in Vibration-Assisted Rotary Drilling – finite element modeling with analytical validation. *ASME Journal of Resources Technology*, vol. 135, issue 3.

Halsey, G. W. et al. (1988). *Torque feedback used to cure slip-stick motion*. SPE Drilling Conference, Houston, Texas, USA.

Han, G. et al. (2006). *Percussion drilling: From laboratory tests to dynamic modeling*. SPE International Oil and Gas conference, China.

Hutchinson, J. R. (2000). *Shear coefficient for Timoshenko beam theory*. ASME Journal of Applied Mechanics, vol. 68, issue 1.

Ibrahim, A. et al. (1987). Modeling of the dynamics of a continuous beam including nonlinear fatigue crack. *International Journal of Analytical and Experimental Modal Analysis*, vol. 2 (2), 76-82.

Jardine, S. et al. (1994). Putting a damper on drillings bad vibration. *Oilfield Review*, vol. 12, 15-20.

Jansen, J. D. (1991). Nonlinear rotor dynamics as applied to oil well drillstring vibrations. *Journal of Sound and Vibration*, vol. 147 (1), 115-135.

Jogi, P. N. et al. (2002). *Field verification of a model-derived natural frequencies of a drillstring*. ASME Energy Sources Technology conference, U.S.A.

Karnopp DC, Margolis DL and Rosenberg RC. *System dynamics: modeling and simulation of mechatronic systems*. 4th edition. New Jersey: John Wiley & Sons Inc., 2006.

Khulief, Y. A. et al. (2008). Vibration analysis of drillstrings with string-borehole interaction. *Journal of Mechanical Engineering Science (ImechE)*, vol. 222, 2099-2110.

Khulief, Y. A. et al. (2009). Laboratory investigation of drillstring vibrations. *Journal of Mechanical Engineering Science (ImechE)*, vol. 223, 2249-2262.

Kreisle, L. F. (1970). Mathematical analysis of effect of shock sub on the longitudinal vibrations of an oil well drillstring. *Society of Petroleum Engineers Journal*, vol. 10, No. 4, 349-356.

Kriesels, P. C. et al. (1999). *Cost saving through an integrated approach to drillstring vibration control*. SPE/IADC Middle East Drilling Technology conference, Abu Dhabi, UAE.

Leine, R. I. et al. (2002). Stick-slip whirl interaction in drillstring dynamics. *Journal of Vibration and Acoustics*, vol. 124, 209-220.

Lin, Y. Q. et al. (1991). Stick-slip vibrations of drillstrings. *Journal of Engineering for Industry, ASME transaction*, 113, 38-43.

Navarro-Lopez, E. M. et al. (2007). Avoiding harmful oscillations in a drillstring through dynamical analysis. *Journal of Sound and Vibration*, vol. 307, 152-171.

Rao, J. S. (1992). *Advanced theory of vibrations*. New Delhi: Wiley eastern limited.

Sananlkone, P et al. (1992). *A field method for controlling drillstring torsional vibrations* SPE Drilling conference, New Orleans, USA.

Shuttleworth, N. E. (1998). *Revised drilling practices, VSS-MWD tool successfully addresses catastrophic bit/drillstring vibration*. IADC/SPE Drilling conference, Texas, USA.

Spanos, P. D. et al. (1992). *Advances in dynamic bottomhole assembly modeling and dynamic response determination*. IADC/SPE Drilling conference, U.S.A.

Spanos, P. et al. (1995). Modeling of roller cone bit lift-off dynamics in rotary drilling. *Journal of Energy Resources Technology,* vol. 117(2), 115-124.

Thomsen, J. J. (2003). *Vibrations and stability* (2nd ed.*)*. Berlin: Springer publishing Co.

Wiercigroch, M. et al. (2008). Vibrational energy transfer via modulated impacts for percussive drilling. *Journal of Theoretical and Applied Mechanics*, vol. 46(3), 715-

726.

Yigit, A. S. et al. (1996). Coupled axial and transverse vibrations of oil well drillstrings. *Journal of Sound and Vibration*, vol. 195 (4), 617-627.

Yigit, A. S. et al. (1998). Coupled Torsional and bending vibrations of drillstrings subject to impact with friction. *Journal of Sound and Vibration*, vol. 215 (1), 167-181.

Yigit, A. S. et al. (2006). Stick-slip and bit-bounce interaction in oil well drillstrings. *Journal of Energy Resources Technology*, vol. 128, 268-274.

Zamanian, M. et al. (2007). Stick-slip oscillations of drag bits by considering damping of drilling mud and active damping system. *Journal of Petroleum Science and Engineering*, vol. 59, 289-299.

Zifeng, L. et al. (2007). *Analysis of longitudinal vibration of drillstring in air and gas drilling*. SPE rocky mountain oil & gas technology symposium, U.S.A.

20-Sim v.4.1, (2010) Controllab Products B.V., Enschede, Netherlands.

Appendix A: Equations of each block in the bond graph modeling

MGY Block:

variables

real global I_Collar[3,3];

real W[3, 3];

equations

W[1, 1] = 0;

W[1, 2] = -P.f[3];

W[1, 3] = P.f[2];

W[2, 1] = P.f[3];

W[2, 2] = 0;

W[2, 3] = -P.f[1];

W[3, 1] = -P.f[2];

W[3, 2] = P.f[1];

W[3, 3] = 0;

P.e = W × I_Collar × P.f;

Cardan01 Block:

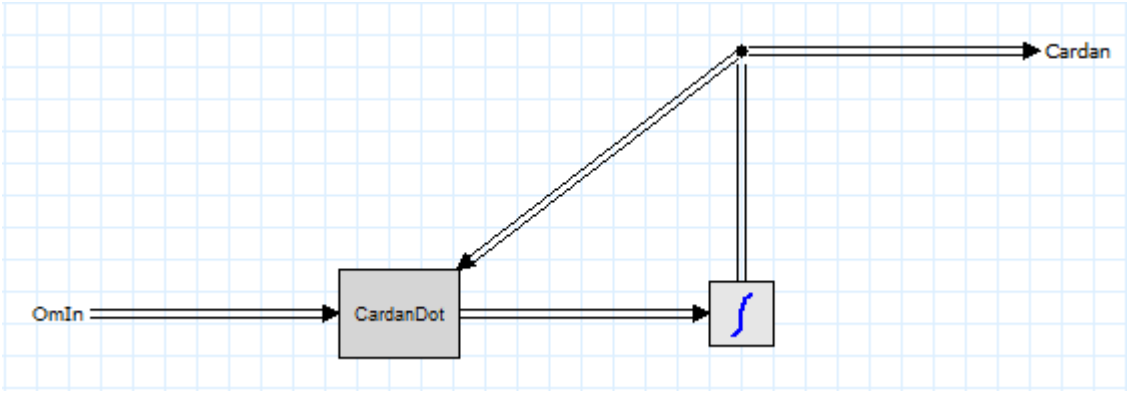

CardanDot Block:

variables

```
real    costh;
real    sinth;
real    tanth;
real    cospsi;
real    sinpsi;
real    B[3, 3];
```

equations

```
costh = cos(Cardan[2]);
sinth = sin(Cardan[2]);
tanth = sinth / costh;
cospsi = cos(Cardan[3]);
```

sinpsi = sin(Cardan[3]);

B[1, 1] = cospsi / costh;

B[1, 2] = -sinpsi / costh;

B[1, 3] = 0;

B[2, 1] = sinpsi;

B[2, 2] = cospsi;

B[2, 3] = 0;

B[3, 1] = -cospsi × tanth;

B[3, 2] = sinpsi × tanth;

B[3, 3] = 1;

CardanDot = B × Omega;

XA11 and XB11 Blocks:

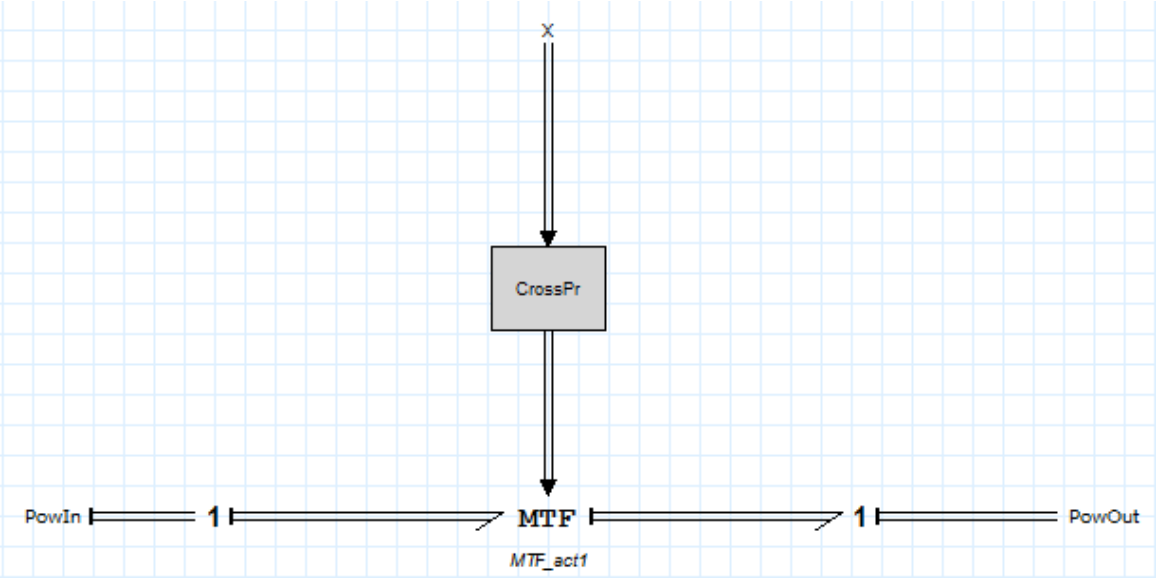

CrossPr Block:

equations

Fmt[1, 1] = 0;

Fmt[1, 2] = X[3];

Fmt[1, 3] = -X[2];

Fmt[2, 1] = -X[3];

Fmt[2, 2] = 0;

Fmt[2, 3] = X[1];

Fmt[3, 1] = X[2];

Fmt[3, 2] = -X[1];

Fmt[3, 3] = 0;

Trans01 Block:

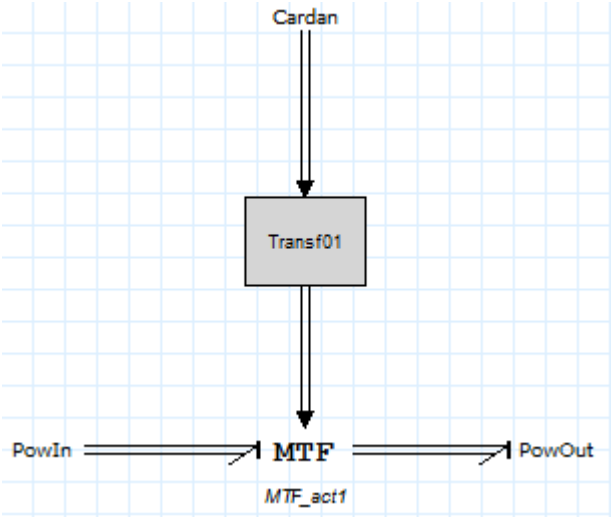

Transf01 Block:

variables

real cphi;

real sphi;

real cth;

real sth;

real cpsi;

real spsi;

real R[3,3];

equations

```
cphi = cos(CAng[1]);
sphi = sin(CAng[1]);
cth = cos(CAng[2]);
sth = sin(CAng[2]);
cpsi = cos(CAng[3]);
spsi = sin(CAng[3]);
A[1, 1] = cth × cpsi;
A[2, 1] = cphi × spsi + sphi × sth × cpsi;
A[3, 1] = sphi × spsi - cphi × sth × cpsi;
A[1, 2] = -cth × spsi;
A[2, 2] = cphi × cpsi - sphi × sth × spsi;
A[3, 2] = sphi × cpsi + cphi × sth × spsi;
A[1, 3] = sth;
A[2, 3] = -sphi × cth;
A[3, 3] = cphi × cth;
R = A×[1, 0, 0;0, 0, -1;0, 1, 0];
```

MTF (fix to inertia) Block:

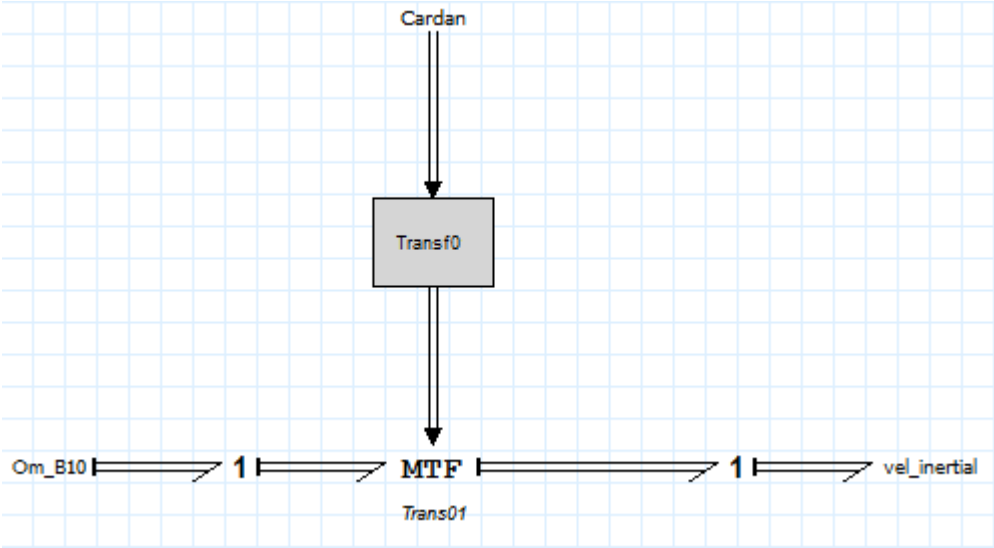

Transf0 Block:

variables

real A[3,3];

real cphi;

real sphi;

real cth;

real sth;

real cpsi;

real spsi;

equations

cphi = cos(CAng[1]);

sphi = sin(CAng[1]);

cth = cos(CAng[2]);

sth = sin(CAng[2]);

```
cpsi = cos(CAng[3]);
spsi = sin(CAng[3]);
A[1, 1] = cth × cpsi;
A[2, 1] = cphi × spsi + sphi × sth × cpsi;
A[3, 1] = sphi × spsi - cphi × sth × cpsi;
A[1, 2] = -cth × spsi;
A[2, 2] = cphi × cpsi - sphi × sth × spsi;
A[3, 2] = sphi × cpsi + cphi × sth × spsi;
A[1, 3] = sth;
A[2, 3] = -sphi × cth;
A[3, 3] = cphi × cth;
B = A;
```

MTF (body1_body2) Block:

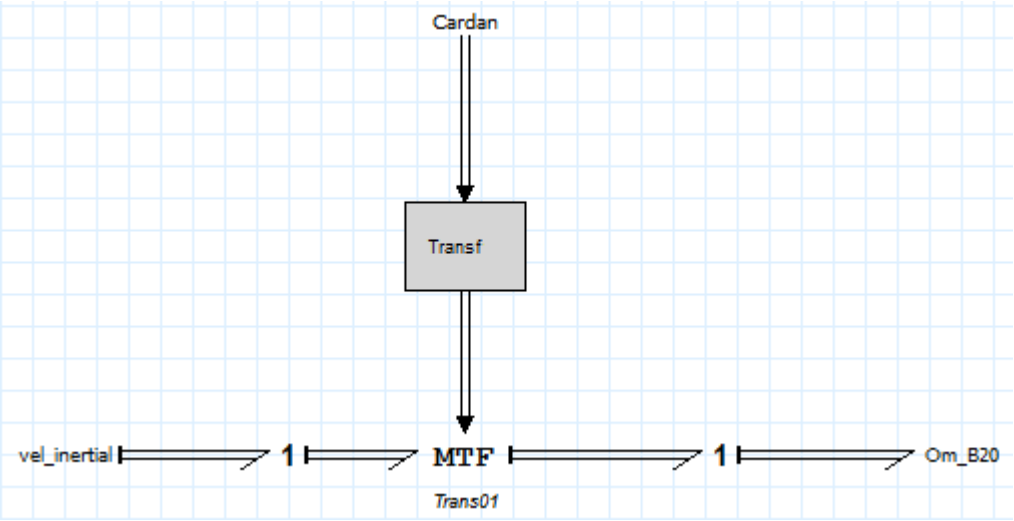

Transf Block:

variables

real A[3,3];

real cphi;

real sphi;

real cth;

real sth;

real cpsi;

real spsi;

equations

cphi = cos(CAng[1]);

sphi = sin(CAng[1]);

cth = cos(CAng[2]);

sth = sin(CAng[2]);

```
cpsi = cos(CAng[3]);

spsi = sin(CAng[3]);

A[1, 1] = cth × cpsi;

A[2, 1] = cphi × spsi + sphi × sth × cpsi;

A[3, 1] = sphi × spsi - cphi × sth × cpsi;

A[1, 2] = -cth × spsi;

A[2, 2] = cphi × cpsi - sphi × sth × spsi;

A[3, 2] = sphi × cpsi + cphi × sth × spsi;

A[1, 3] = sth;

A[2, 3] = -sphi × cth;

A[3, 3] = cphi × cth;

B = transpose(A);
```